Quantitative aspects of gas-phase metal ion chemistry: Conservation of spin, participation of f orbitals, and C-H activation and C-C coupling

P. B. Armentrout*

Department of Chemistry, University of Utah, Salt Lake City, UT 84112, USA

Abstract. In this feature article, I reflect on over 40 years of guided ion beam tandem mass spectrometry (GIBMS) studies involving atomic metal cations and their clusters throughout the periodic table. Studies that have considered the role of spin conservation (or lack thereof) are a primary focus, with a quantitative assessment of the effects examined. A need for state-specific studies of heavier elements is noted as is a more quantitative assessment of spin-orbit interactions in reactivity. Because GIBMS experiments explicitly evaluate the kinetic energy dependence of reactions over a wide range, several interesting and unusual observations are highlighted. More detailed studies of such unusual reaction events would be welcome. Activation of C-H bonds and ensuing C-C coupling events are reviewed, with future work encouraged. Finally, studies of lanthanides and actinides are examined with an eye on understanding the role of *f* orbitals in the chemistry, both as participants (or not) in the bonding and as sources/sinks of electron density. This area seems ripe for more quantitative experiments.

*Corresponding author. email: armentrout@chem.utah.edu

Introduction

In 1979, building on previous studies of alkyl halides and alcohols,[1, 2] Allison, Freas, and Ridge observed C-H and C-C bond activation of iso- and n-butane by atomic *3d* transition metal cations (Fe^+, Co^+, Ni^+, and Ti^+).[3] As they noted then, the only other report of C-C bond activation in alkanes was limited to a study of vaporized nickel with pentane, where the active species could not be identified but was likely small nickel clusters.[4] The former gas-phase observation set off a flurry of activity to further characterize how atomic metal ions could activate alkanes, some of the most inactive molecules of technological interest. Another key observation was made by Irikura and Beauchamp, who found that several of the *5d* transition metal cations (W^+, Ta^+, Os^+, Ir^+, and Pt^+) could activate methane at room temperature,[5-7] whereas none of the *3d* and *4d* metals can do so. (Although Zr^+ is reported to dehydrogenate methane at thermal energies, the reaction is inefficient, <1% of the collision limit,[8] and later studies showed the reaction is endothermic by 0.11 eV.[9]) Several reviews have nicely summarized many of the key findings of the many subsequent studies on gas-phase metal ion chemistry with alkanes.[10-17]

At about the same time, Smalley, Bondybey, and co-workers developed laser vaporization/supersonic expansion sources to produce metal clusters.[18, 19] A similar explosion of studies ensued.[20-24] These experiments have evolved to include catalysis by clusters[25] and even single atoms[26] deposited on substrates. Such deposited species can begin to realize true catalytic behavior and the utility of gas-phase atomic and cluster results is increased by quantitative comparisons with such studies.

As a long-term participant in studies of both atomic metal ions (starting in 1977)[27] and their clusters (starting in 1984),[28] in this feature article, I reflect on over four decades of wide-ranging research and highlight some of the things that have been learned and some that are still to be discovered.

Experimental approach

Experimental details of our guided ion beam tandem mass spectrometry (GIBMS) studies and the interpretation of the kinetic energy resolved cross sections that result can be found in the original papers cited below and in several reviews.[29-32] Included here is a very brief description of these methods.

Figure 1 shows a schematic of one of our GIBMS instruments. Functionally, such an apparatus comprises five main sections: an ion source, an initial mass spectrometer (MS), a reaction region that incorporates a radio frequency (rf) ion guide, a second MS, and an ion detector. As will be seen below, the ion source can be one of many different types, but for quantitative GIBMS studies, it *must* be able to produce ions with a known distribution of internal and kinetic energies. In that regard, it is much more important that the temperature of the ions be known than it is for them to be cold. For a particular experiment, a single mass is selected by the initial MS so that the desirable MS attributes are efficient transmission and high mass resolution. Therefore, we utilize a magnetic sector in both instruments. For the second mass analysis MS, we have used a quadrupole mass filter as it permits rapid scanning of the mass, effective mass transmission (which is essential to accurately measure the absolute reaction probabilities), and reasonable mass resolution (which is generally sacrificed when needed to ensure good transmission). A time-of-flight MS would be an alternative choice for the analysis MS, but ensuring no mass bias in the collection would be important. Both of our instruments also utilize a Daly-type scintillation detector[33] (with a high voltage 22 – 25 kV first dynode) as this affords excellent signal and near unity detection efficiency for the mass range covered.

The key aspect of a GIBMS instrument is the use of an ion guide in the interaction region where the neutral gas reactant is introduced in a gas cell. It might be appreciated that at the time we constructed our first apparatus, the octopole ion guide had been developed by Ernst Teloy and Dieter Gerlich[34] and Gerlich had brought the technology to Yuan Lee's laboratory.[35] My laboratory was therefore the third to utilize this valuable technique, aided considerably by Lee's student Scott Anderson, who had worked with Dieter and continued to perform experiments on that apparatus. As in those early instruments, we chose an ion guide with eight rods (an octopole) as it was fairly

straightforward to build and assemble and its effective trapping voltage has a $1/r^6$ radial dependence that does not perturb the kinetic energies of the ions greatly (unlike quadrupole guides).[36] One important aspect of the ion guide is that its radial trapping permits the ion energy to be very low, essentially thermal, whereas without trapping, energies below about 1 volt would lead to loss of the ion signal. This ability also allows the distribution of ion kinetic energies as well as the zero of the energy scale to be routinely measured using a retarding technique.[37] By changing the voltage difference between the source and the dc bias on the octopole, the ion kinetic energy can be varied over about four orders of magnitude. This ability is the truly distinguishing aspect of GIBMS experiments for exploring ion-molecule chemistry, as described below.

Probably the other key development in the projects described below was the mathematical description of how reaction cross sections depend on energy. Early experiments in my laboratory explored a number of simple forms to model this kinetic energy dependence. Eventually, we settled on the modified line-of-centers (MLOC) model that has proven to be robust. This simple form can then be augmented with additional terms that allow it to describe a very wide range of reactions.[38-40] A key experiment also enabled us to directly relate this model to the energy deposition function,[41] i.e., how much energy is transferred from translational to internal degrees of freedom during a collision. Again more detailed descriptions of the model, its evolution, and its rationale can be found in previous articles and reviews.[30, 38-40, 42]

Is spin a good quantum number for metals?

First-row transition metals. Much of the early work conducted in my group was focused on reactions of specific electronic states of atomic *3d* transition metal cations, which could be isolated by combining experiments that generated the ions using surface ionization (SI), electron ionization (EI), and a high-pressure drift cell source (DC)[43] (and later, a flow tube source).[44, 45] For example, we showed that the reaction of ground state Fe^+ (^6D, $4s^13d^6$) with H_2, HD, and D_2 (endothermic by about 2 eV) was 68 times less efficient than the reaction of the excited state, Fe^+ (^4F, $3d^7$), even though this state lies only 0.25 eV higher in energy (average over all spin-orbit

levels). Notably, both reactions are spin-allowed because they form ground state FeH^+ ($^5\Delta$) + H (^2S).[46, 47] Furthermore, the two electronic states exhibit completely distinct branching ratios in the reaction with HD, indicating very different reaction mechanisms. Both the relative reaction efficiency and the HD branching ratios can be understood on the basis of the orbital occupations, namely, the occupied versus empty *4s* orbital.[43] In these studies, there is no experimental evidence that the surfaces evolving from these two electronic asymptotes interact, i.e., surfaces evolving from the ^6D state do not couple with those from the ^4F state in order to enhance their reactivity. Furthermore, the enhanced reactivity of the excited state is not a consequence of the additional electronic energy. This is conclusively demonstrated by the observation that ground state Ni^+ (^2D, $3d^9$) is much more reactive than the excited state Ni^+ (^4F, $4s^13d^8$).[48] Again, these differences can be understood on the basis of the electron configurations.

We then examined reactions of the same two states of Fe^+ with propane[49] and later methane and ethane.[50] For the endothermic reactions observed (both C-H and C-C cleavages), the excited ^4F state remained much more reactive than the ^6D state. However, both ethane and propane have exothermic reaction channels: dehydrogenation in both cases and elimination of methane in the latter case, such that iron cation alkene complexes are formed. Even though barrierless, these exothermic reactions are only modestly efficient, about 20% of the Langevin-Gioumousis-Stevenson collision cross section, σ_{LGS}, at the lowest energy (near thermal).[51, 52] For these reactions, the ^6D state is equally or more reactive at low collision energies (below ~0.5 eV), but switches at higher energies such that the ^4F state is again much more reactive, as seen in Figure 2. (Later, spin-orbit selected experiments by Weisshaar and co-workers indicate that the ^4F state remains more reactive than ^6D by a factor of two at an energy of 0.24 eV and a factor of four at 1.0 eV collision energy. Once the distributions of J levels are considered, these results are within experimental uncertainty of the GIBMS results, which have large uncertainties at the lowest energies, Figure 2. They also found that the $^4F_{5/2}$ level is about twice as reactive as $^4F_{7/2}$ and $^4F_{9/2}$.[53, 54]) At the time of these studies, which was before the advent of routine *ab initio* calculations, we constructed a qualitative potential energy surface from first principles, Figure 3. Because the

inserted intermediates needed for C-H and C-C bond activation, H-Fe^+-R or H_3C-Fe^+-R where R could be H, CH_3, C_2H_5, or C_3H_7, had to have quartet spin (in order for there to be two covalent bonds to iron), there had to be a crossing between the sextet spin surfaces evolving from Fe^+ (^6D) and the quartet surfaces from Fe^+ (^4F) that lead to products. We hypothesized that the reactivity of the ^6D state at low energies occurred because spin was no longer conserved and the sextet reactants followed the adiabatic pathway to form quartet intermediates (full lines in Figure 3). At higher energies, non-adiabatic spin-conserving behavior (dashed lines) becomes more probable and coupling of the sextet surfaces to the reactive quartet spin state surfaces decreases. We commented that "we expect that these crossings are ubiquitous in ionic and neutral transition metal reactions." Although prior studies had suggested such phenomena,[29, 43, 55-58] to my knowledge, this was the first clear experimental demonstration of "two-state reactivity" later coined and touted by Schroder, Shaik, and Schwarz as a "New Concept in Organometallic Chemistry".[59, 60] For the *3d* transition metal atomic ions, these studies suggest that spin appears to be a reasonably good quantum number but needs not be rigorously conserved, especially at low collision energies when the reactants have sufficient time to explore the electronic landscape. Additional details about the potential energy surface for the Fe^+ + propane reaction were later obtained by collisional activation of the $Fe^+(C_3H_8)$ intermediate[61] and by isotope labeling and kinetic energy release distribution experiments.[62] Later theoretical calculations confirm the major aspects (especially the curve crossing) of the qualitative potential energy surface originally suggested, although details of some steps were adjusted.[63]

Third-row transition metal ions. In metal chemistry, the question then arises whether spin conservation becomes less of a concern as one moves down the periodic table. In a review "On the spin-forbiddeness of gas-phase ion-molecule reactions," Schwarz noted "There is actually a continuum of 'forbiddeness' being largest when the affected electrons are localized on light atoms, such as first row elements and much less so for the heavier *4f*, *5d* and *5f* elements."[64] In their seminal study of the *5d* transition metal cations activating methane,[6] Irikura and Beauchamp opined "strong spin-orbit coupling in the heavy metals weakens the validity of basic concepts such

as total spin and electron configuration." Indeed, my group has demonstrated that for several of the *5d* metal cation reactions, spin conservation can be quite weak. A notable example is the endothermic dehydrogenation of methane by Re^+ (^7S),[65] with the results shown in Figure 4. On the basis of *ab initio* calculations, Figure 5, we found "dehydrogenation of methane by Re^+ appears to require three spin changes along the lowest energy path available: Re^+ (^7S) + CH_4 ($^1A_1$) → H–Re^+–CH_3 ($^5A'$) → $(H)_2ReCH_2^+$ (^3A) → $(H_2)ReCH_2^+$ ($^5B_1$) → $ReCH_2^+$ ($^5B_1$) + H_2 ($^1\Sigma_g^+$). Despite this requirement, the reaction is found to occur with high efficiency [86 ± 10%], suggesting that spin-conservation is not an impediment for reaction of this heavy metal system." Thus, this study provides some quantitative measure of how efficient the coupling between surfaces of different spin must be for a heavy metal.

However, what about the converse? If the system were to start on the excited state surface, is the spin-orbit coupling sufficiently complete that the system will remain on the excited surface and not drop down to the ground state adiabatic surface? Some evidence that the system does not remain on the adiabatic surfaces comes from the same study.[65] Here, a small amount of electronically excited states of Re^+ is observed to undergo exothermic dehydrogenation of methane, Figure 4 (open symbols). The excited states must lie above 0.57 ± 0.06 eV (the endothermicity of the dehydrogenation reaction) and below 2.4 eV (the endothermicity of formation of ReH^+), which therefore includes several excited states of quintet spin starting at 1.7 eV excitation.[66] This exothermic reaction occurs with an efficiency of only 0.08% compared with the LGS collision cross section. This overall reaction efficiency includes both the amount of excited state present *and* the efficiency of the coupling between adiabatic surfaces. Because the former is not known quantitatively, the latter cannot be determined.

Kinetic energy dependence. It can be realized that the coupling between surfaces is dependent on the kinetic energy at the surface crossing. The ability of GIBMS to examine the kinetic energy dependence of reactions over a wide range has enabled us to measure this explicitly on several occasions. One of the first clear examples was our study of the reactions of V^+ (^5D) with CS_2 and COS forming VS^+.[67] (Earlier examples showing many of the same features described here

occur for the reactions $S^+ + H_2 \rightarrow SH^+ + H$,[68] $M^+ + CO_2 \rightarrow MO^+ + CO$ where M = V[69] and Nb,[70] and later examples include $M^+ + COS \rightarrow MS^+ + CO$ where M = Cr, Mn,[71] Fe, and Co.[72]) Because D_0(S-CS) = 4.50 ± 0.02 eV[73-75] > D_0(V^+-S) = 3.72 ± 0.09 eV[67, 76] > D_0(S-CO) = 3.17 ± 0.02 eV,[73-75] formation of ground state VS^+ ($^3\Sigma^-$) is endothermic in the reaction with CS_2 and exothermic with COS. In the latter reaction, the cross section for the VS^+ + CO product channel is barrierless, but rather than declining with collision energy (E) as predicted by the LGS collision cross section, namely as $E^{-1/2}$, it rather declines approximately as $E^{-1.0}$. (Figure 2 also shows this behavior for the $Fe^+ + C_3H_8$ system.) In the CS_2 reaction, the VS^+ + CS cross section exhibits a threshold providing the endothermicity of the reaction (from which the VS^+ bond energy was determined), but also peaks at a low energy near 1.2 eV, Figure 6. Ordinarily, cross sections for such a simple exchange reaction are found to peak at the bond energy of the bond being broken in the neutral (here, S-CS) because this is where there is enough energy that the ionic product can begin to dissociate, thereby leading to a decrease in the formation of stable product. Clearly, 1.2 eV is well below D_0(S-CS) = 4.50 eV, such that some other factor is influencing the shape of the cross section. Modeling the data using a modified line-of-centers (MLOC) approach[30-32] demonstrated that the addition of an $E^{-1/2}$ factor in the model was able to reproduce the data effectively, as shown in Figure 6.

Also displayed in Figure 6 is the observation of a distinct feature in the cross section at higher energies that does reach a maximum near D_0(S-CS). The COS reaction similarly showed an increase in the formation of VS^+ starting at an energy near 0.9 eV, such that the threshold is shifted down from that in Figure 6 by an amount consistent with the difference in the bond energies of CS_2 and COS (1.3 eV). At the time, this observation was relatively unusual in GIBMS experiments, although we had seen similar effects in other systems[68-70] and several related systems since (see below). This led us to suggest that "the routes to the two products in question must differ in some fundamental way." Because *ab initio* calculations[76] had predicted a $^3\Sigma^-$ ground state for VS^+ with the first quintet state ($^5\Pi$) lying 1.37 eV higher in energy, we suggested that the two cross section features could be attributed to formation of the two VS^+ electronic states. The "fundamental" difference between these two processes is that formation of ground state products

from ground state reactants in reaction 1 is spin-forbidden, whereas formation of the excited state in reaction 2 is spin-allowed.

$$V^+ (^5D) + CS_2 (^1\Sigma^+_g) \rightarrow VS^+ (^3\Sigma^-) + CS (^1\Sigma^+) \quad (1)$$

$$\rightarrow VS^+ (^5\Pi) + CS (^1\Sigma^+) \quad (2)$$

Similarly, the reaction with COS leads to an exothermic and an endothermic feature in the cross section for the same reason.

The additional $E^{-1/2}$ energy dependence observed at low energy may therefore be attributable to the spin-forbidden nature of reaction 1 and its COS analogue, likewise for $Fe^+(^6D) + C_3H_8$. *Ab initio* calculations of the potential energy surface for the CS_2 system suggested that the minimum energy crossing point (MECP) between the quintet and triplet surfaces lay near -0.6 ± 0.1 eV relative to the $V^+ (^5D) + CS_2$ entrance channel. A crude estimate for the spin-orbit coupling constant (H_{SO}) at the MECP geometry was obtained from additional *ab initio* calculations that explicitly treated the different spin-orbit states. Those calculations suggested a coupling constant of ~20 cm^{-1} (0.0025 eV), which lies in the weak-coupling limit.[77]

Simple models that predict the probability of surface crossings include the Landau[78]-Zener[79] (LZ)-Steukelberg[80] model.[81]

$$P_{LZ} = \exp\{-[c/(E - E_C)]^{1/2}\} \quad (3)$$

Here, c is a surface coupling term that depends on the energy gap between the adiabatic curves (2 H_{SO}) and inversely on the difference in the slopes of the diabatic curves at the crossing point, E is the relative kinetic energy of the reactants, and E_C is the potential energy of the crossing point. Eq. 3 describes the probability for a single pass through the avoided crossing region, but as we discussed,[67] the energy dependences for a single, double, or infinite number of passes are all approximately the same when in the weak-coupling limit (small c).

In the Landau-Zener model, the single dimension refers to the relative translational motion of the reactants. For multi-dimensional surfaces, the component of the nuclear velocity perpendicular to the surface-crossing seam, which determines the crossing probability,[77, 82, 83] could be vibrational rather than translational. However, it has been shown that the crossing probability

between diabatic surfaces of different spin multiplicities has an $(E - E_C)^{-1/2}$ dependence for weakly coupled diabatic surfaces regardless of the dimensionality of the hypersurface.[83, 84] Further, vibrationally-coupled, spin-forbidden charge-transfer reactions have been shown to exhibit $E^{-1/2}$ energy dependences.[85] Generally, in our GIBMS experiments, E is essentially the translational energy of the reactants such that the $(E - E_C)^{-1/2}$ energy dependence is a general approximation to the surface-crossing behavior that is appropriate for a variety of crossing mechanisms. Except at very low collision energies, the $(E - E_C)^{-1/2}$ energy dependence can be approximated by $E^{-1/2}$, which matches the general behavior noted for the $V^+ + CS_2$ and COS and $Fe^+ + C_3H_8$ reactions. In the former study, various values of c and E_C were tested and the results were insensitive to these variations. We concluded that "as long as the spin-forbidden process exhibits a power-law energy dependence, the empirical modeling appears to be capable of providing a reliable estimate of the energy threshold, certainly within any typical experimental error." Clearly the model accurately reproduces the observed cross sections as well, Figure 6.

As noted above, observations similar to this have now been made for a number of heavy element systems, where one might imagine that the spin-orbit coupling constant is higher (although this has not been calculated theoretically). In particular, we have observed this behavior for the reactions of several ground state lanthanide cations (Ln^+) (Ln = Gd,[86, 87] Nd,[88] and Pr[89]) with CO_2, isoelectronic with CS_2 and COS. The oxidation of the metal cation by CO_2 leads to the formation of $LnO^+ + CO$. Because multiple covalent bonds are formed between Ln^+ and O (just as for V^+ and S), the spin state of ground LnO^+ is generally lower than that of the ground state of Ln^+, such that the adiabatic reaction is spin-forbidden and there is a spin-allowed process that occurs at higher energies. As for the $V^+ + COS$ reaction, this leads to a cross section for LnO^+ formation that exhibits exothermic, barrierless behavior at low energies and then an increase in the cross section at higher energies. For all three Ln^+ systems, the cross sections at low energies decrease as E^{-1}. We conclude that even though these heavy element systems should have higher spin-orbit coupling constants than the vanadium system, the qualitative dependence on velocity ($E^{-1/2}$) seems to be maintained. Furthermore, even though spin clearly needs *not* be conserved, spin conservation does

appear to influence the probability of the reactions, with spin-conserving reactions being more probable, at least at high collision energies.

Are there other adiabaticities/diabaticities besides spin?

Plane of symmetry. Conservation of spin provides a useful paradigm for understanding the unusual kinetic energy dependence of the systems described above; however, we have also observed similar cross section features in systems where spin conservation cannot be an issue. Figure 7 shows the example of Os^+ (^6D) + O_2 ($^3\Sigma_g^-$) → OsO^+ + O (^3P).[90] Similar behavior has also been observed for reactions of Re^+ (^7S) + O_2[91] and more subtly for Ir^+ (^5F) + O_2.[92] In all these systems, because the neutral reactants and products have triplet spin states, a manifold of MO^+ electronic states can be formed by spin-allowed pathways. In the case of Os^+, the reactants can evolve along potential energy surfaces having quartet, sextet, and octet spin (s = 3/2, 5/2, 7/2, respectively) depending on how the unpaired electrons in the two reactants couple. Because the neutral product is also triplet spin, the intermediates can form OsO^+ products having doublet, quartet, sextet, octet, and dectet spin (s = 1/2, 3/2, 5/2, 7/2, and 9/2, respectively). In the case of OsO^+, we calculated that the ground state was either $^6\Sigma^+$, $^4\Pi$, or $^4\Phi$ (all lying within 0.1 eV of one another), with $^4\Pi_{5/2}$ being favored once spin-orbit corrections were made. Subsequent calculations by Liu et al. support this assignment.[93] Clearly, formation of OsO^+ ($^6\Sigma^+$) is spin allowed from ground state reactants, but so are the $^4\Pi$ and $^4\Phi$ states. Thus, the spin-forbidden reaction at low energies and spin-allowed reaction at higher energies can no longer provide a rationale for the two features observed in the reactions of Os^+ with O_2, and similarly for Re^+ and Ir^+.

When we first published these results, we also considered whether the two features might result from excited state M^+ reactants or the formation of excited state O (^1D), but these possibilities could be eliminated in all three systems by varying source conditions and a quantitative comparison of the energies. We also considered the nature of the potential energy surfaces in the entrance channel where the O_2 bond is activated by insertion of the metal cation. For Os^+ (^6D), 60% of the surfaces have A′ (in-plane) symmetry and 40% have A″ (out-of-plane)

symmetry. Low-energy (lying below the energy of the reactants) pathways were found along both $^6A'$ and $^4A'$ ($^4B_2$) surfaces leading to stable OsO_2^+ intermediates ($^2A_1$ ground state and $^4B_2$ and $^6A_1$ states). We imagine that at low kinetic energies, the reactants pass slowly through the crossing regions, which allows spin inversion to be efficient and adiabatic behavior to ensue. In contrast, surfaces having A″ symmetry have no low-energy pathways and all surfaces exhibit some type of barrier in the entrance channel. Thus, a plausible explanation for the two cross section features observed experimentally is that the low-energy behavior corresponds to reactions along the A′ surfaces, which then decline as the energy gets higher, perhaps because spin-forbidden crossings are needed or because the system becomes increasingly diabatic as the energy gets higher. The high-energy cross section feature observed experimentally could then be associated with reactions along the A″ surfaces with possible contributions from mixing A′ and A″ surfaces via Coriolis coupling. Coriolis coupling, a breakdown in the Born-Oppenheimer approximation where the electronic motion lags out of the plane because of the fast rotation of the molecule, can occur at high energy as identified in previous studies of Ar^+ /Kr^+ /Xe^+ + H_2/D_2/HD reactions at energies above 1–2 eV.[37, 94, 95] For the M^+ + O_2 systems, the Re^+ and Ir^+ systems displayed similar differences between the A′ and A″ surfaces in the entrance channel, such that parallel explanations hold.

To further explore whether the plane-of-symmetry explanation was viable, we pursued several additional experiments. We first examined the oxidation reactions of these three metals with CO ($^1\Sigma^+$).[96] As for the reaction with O_2, these triatomic reactions can evolve along both A′ and A″ surfaces. Because this reactant has singlet spin, reactions that conserve spin are more restricted than in the O_2 systems; however, because the C (^3P) atom neutral product still has triplet spin, multiple spin states of the MCO^+ intermediate remain accessible. Thus, spin-allowed pathways to form ground state MO^+ are available for Os^+ and Ir^+, but formation of ReO^+ ($^3\Delta$) is spin-forbidden from Re^+ (^7S). Despite this, ground state products were observed at their thermodynamic thresholds in all three systems and only one cross section feature was observed, Figure 7. The latter observation was attributed to the high kinetic energies needed to break the very

strong CO bond (11.11 eV[75]) and form MO^+. Because the reactions are endothermic by over 6 eV, all calculated potential energy surfaces lie below the product energies such that there are no surfaces with excess barriers, unlike the O_2 systems where the endothermicities are small.

We next pursued the oxidation reactions with SO_2 with all three metal cations.[97-99] This oxidant has a singlet spin ground state and yields a SO neutral product with a triplet ground state, such that the spin restrictions are the same as for the reactions with CO. Further, $D_0(O–SO) = 5.66$ eV[75] is similar to $D_0(O_2) = 5.117$ eV thereby minimizing any thermodynamic differences in the behavior of these two systems. For all three metal cations, the reactions with SO_2 exhibit only a single cross section feature, Figure 7. In contrast to the $M^+ + O_2$ and CO triatomic systems, the four atom $M^+ + SO_2$ systems no longer have a plane of symmetry constraining their reactions, such that there is no distinction between A′ and A″ symmetries, consistent with the absence of two features in the SO_2 systems. We concluded that the two endothermic features found in the $M^+ + O_2$ reactions is plausibly explained by the plane-of-symmetry argument.

Orbital diabaticity. Although an example of the phenomenon discussed in this section has not been recognized for metal ion chemistry, I believe that this is because there is yet insufficiently quantitative information available to allow its identification. This additional possible constraint on reaction systems has been observed for dissociation of protonated hydrazine, $N_2H_5^+$.[100] The identification of the observed effect relies on the fact that the energetics of the processes are very well known, unlike the situation for any system involving metals. Collision of $N_2H_5^+$ (and the perdeuterated version) with Xe leads to homolytic N-N bond cleavage and the formation of $NH_3^+ + NH_2$ followed at higher energies by heterolytic bond cleavage to yield $NH_2^+ + NH_3$. The threshold energy for the former product (average of the results from the perprotiated and perdeuterated systems after zero-point energy corrections) was determined as 5.10 ± 0.18 eV, which agrees well with reaction 5 but not the much lower energy reaction 4.

$$N_2H_5^+ (^1A') + Xe \rightarrow NH_3^+ (^2A_2'') + NH_2 (^2B_1) + Xe \qquad 3.58 \pm 0.03 \text{ eV} \qquad (4)$$

$$\rightarrow NH_3^+ (^2A_2'') + NH_2 (^2A_1) + Xe \qquad 5.01 \pm 0.03 \text{ eV} \qquad (5)$$

It can be seen that both of these reactions conserve spin, which means the failure to observe reaction 4 is a consequence of some other constraint. Likewise, the threshold measured for NH_2^+ formation was 5.96 ± 0.22 eV, which agrees with reaction 7 but not the lower energy reaction 6.

$$N_2H_5^+ (^1A') + Xe \rightarrow NH_2^+ (^3B_1) + NH_3 (^1A_1) + Xe \qquad 4.57 \pm 0.03 \text{ eV} \qquad (6)$$

$$\rightarrow NH_2^+ (^1A_1) + NH_3 (^1A_1) + Xe \qquad 5.83 \pm 0.03 \text{ eV} \qquad (7)$$

Here, the explanation for the failure to observe reaction 6 may simply be spin conservation.

Theoretical calculations of the various potential energy surfaces for the products of reactions 4 – 7 indicate that the $N_2H_5^+$ ($^1A'$) molecule diabatically dissociates to the products of reaction 7, the highest energy asymptote considered.[100] Thus, formation of any other product combination relies on crossings between diabatic surfaces, which exist for all these pathways. As noted above, reaction 6 is spin-forbidden, and spin is surely a good quantum number for these light atoms. To explain why reaction 5 was observed instead of reaction 4, our theoretical analysis considered the N-N σ bond being broken as well as the lone pair electrons, which have π-like character, such that $N_2H_5^+$ ($^1A'$) has a $\sigma^2\pi^2$ valence configuration. When the σ bond breaks heterolytically in reaction 7, it forms NH_2^+ ($^1A_1$, π^2) + NH_3 ($^1A_1$, σ^2), which conserves the $\sigma^2\pi^2$ orbital occupation. When the σ bond breaks homolytically, formation of NH_3^+ ($^2A_2''$, σ^1) + NH_2 ($^2B_1$, $\sigma^2\pi^1$) in reaction 4 does not conserve the orbital occupation, whereas formation of NH_3^+ ($^2A_2''$, σ^1) + NH_2 ($^2A_1$, $\sigma^1\pi^2$) in reaction 5 does conserve the $\sigma^2\pi^2$ orbital occupation. (Interestingly, for the unobserved reaction 6, formation of NH_2^+ ($^1A_1$, $\sigma^1\pi^1$) + NH_3 ($^1A_1$, σ^2) also does *not* conserve the orbital occupation.) It is important to note that this orbital conservation is certainly influenced by the high energies needed to induce dissociation. This means that the energized $N_2H_5^+$ molecule probably has a short lifetime, which directs the reaction along non-adiabatic (non-Born-Oppenheimer) behavior. Indeed, in mass-analyzed ion kinetic energy spectrometry (MIKES) experiments by Øiestand and Uggerud, the metastable fragments of $N_2H_5^+$ (formed with extensive amounts of internal energy) observed were dominant losses of H_2 and H along with weak loss of NH and homolytic N–N bond cleavage.[101] Nevertheless, the observations made in these GIBMS

experiments may extend to other systems, although the lack of adequate thermochemistry should make such phenomena difficult to identify in many systems.

C-C coupling reactions on metals

Among the observations made by Irikura and Beauchamp in their landmark paper exploring the reactions of the *5d* transition metal cations with methane was oligomerization reactions at room temperature.[7] Ta^+ and W^+ reacted readily to dehydrogenate four methane molecules and the latter with up to eight. Ir^+ reacted rapidly to dehydrogenate two methanes and up to three. Os^+ and Pt^+ reacted efficiently with only a single methane molecule, but dehydrogenation reactions with up to 4 and 5 CH_4 were observed, respectively. Re^+ reacts endothermically with methane (see Figure 4) but $ReCH_2^+$ reacts with an additional three methane molecules. It was presumed on the basis of oxidation state arguments that C-C coupling was involved in the higher order reactions, but no definitive experimental information to justify this has been presented until recently.

Using infrared multiple photon dissociation (IRMPD) action spectroscopy, in collaboration with Bakker, we have examined the products formed by *5d* transition metal cations reacting with methane. Early work established the structures of the primary dehydrogenation products, $[M,C,2H]^+$, as "agostic" MCH_2^+ carbenes for M = Ta and W (in which one CH bond donates its electrons into an empty orbital on M), a classic C_{2v} carbene for Pt, and carbyne hydrides ($HMCH^+$) for Os and Ir, where the latter also generated a small amount of an excited state C_{2v} carbene.[102-104] In addition, IRMPD spectra of $[Au,C,2H]^+$, generated by reaction of Au^+ with oxirane (c-C_2H_4O),[105] identified this species as a carbene, but rather than possessing a covalent double bond, the Au^+-CH_2 bond is a dative double bond, i.e., the lone pair of electrons on CH_2 ($^1A_1$) donates into the empty *6s* orbital of Au^+ (^1S, $5d^{10}$) and there is π-backdonation from Au^+ into the empty 2p orbital on C.[106, 107] (A reviewer comments that the dative designation may be "ambitious". See also refs. [108-110] for additional examinations of this interesting molecule.) Notably, the rotational structure of the observed vibrational bands was an important component of accurately reproducing

the experimentally observed spectra from computational predictions of the vibrational spectrum.[103, 104]

In subsequent studies, we have begun to examine the products formed by sequential reactions with methane. In our first such study,[111] we examined the reactions of Pt^+ in a molecular beam apparatus in which the Pt^+ ions were formed by laser ablation, entrained in a flow of He, exposed to methane in the source channel, and then expanded into vacuum. Product ions had $PtC_nH_{4n-2}^+$ formulae where n = 1 – 4, i.e., only a single dehydrogenation was observed. Comparison of the experimental IRMPD spectra of these species indicated that the n = 2 – 4 species were $Pt(CH_3)_2(CH_4)_{n-2}^+$. Thus, the initially formed $PtCH_2^+$ species reacts with another CH_4 molecule to form the platinum dimethyl cation, which can then adsorb one or two additional methanes. Note that the single dehydrogenation observed is in contrast to the observations of Irikura and Beauchamp, but this difference could be attributed to the high-pressure conditions of the molecular beam versus low-pressure conditions in the ICR experiments. This conclusion was confirmed by later repeating the experiment using a different apparatus operating under low-pressure conditions.[112] Now, both $PtC_2H_4^+$ and $PtC_4H_8^+$ (but no $PtC_3H_6^+$) were observed and shown to have Pt^+(ethene) and $Pt^+(ethene)_2$ structures. Thus, C-C coupling reactions were definitively demonstrated. The failure to observe $PtC_3H_6^+$ (or $PtC_3H_8^+$) suggests that this species reacts rapidly with a fourth methane molecule under our experimental conditions.

Similar experiments have been conducted for Ir^+ reacting with multiple methane molecules. In the molecular beam apparatus, IRMPD spectra were obtained for $[Ir,3C,8H]^+$, $[Ir,3C,10H]^+$, $[Ir,4C,10H]^+$, and $[Ir,4C,12H]^+$.[113] As for Pt^+, the high pressure environment in this experiment suppresses the sequential dehydrogenations that would lead to $[Ir,3C,6H]^+$ and $[Ir,4C,8H]^+$. Comparison of these four spectra to those predicted by theory indicated that these species have structures of $IrCH_2(CH_3)_2^+$, $HIr(CH_3)_3^+$, $Ir(CH_3)_2(C_2H_4)^+$, and a complex mixture of structures, respectively. Notably, evidence of C-C bond coupling is evident for the reactions with four methane molecules. Ongoing experiments conducted at lower pressures find the expected

dehydrogenation products, $[Ir,2C,4H]^+$, $[Ir,3C,6H]^+$, and $[Ir,4C,8H]^+$, which all show evidence of C-C bond formation.

Perhaps our most intriguing recent result is the observation that C-C bond coupling occurs with Ru^+ in a low-pressure environment.[114] This is surprising because the dehydrogenation reaction of Ru^+ with methane is endothermic by 1.14 ± 0.05 eV,[115] which seems like it should shut down the sequential reactions performed at thermal energies. Nevertheless, we observe formation of $[Ru,2C,4H]^+$, identified as the Ru^+ ion with an ethene ligand attached, and $[Ru,4C,6H]^+$, assigned to a $Ru(\eta^4\text{-cis-1,3-butadiene})^+$ complex. Calculations indicate that the barrier toward formation of $Ru(C_2H_4)^+ + 2\ H_2$ is 0.80 eV above the energy of the ground state Ru^+ (^4F) + 2 CH_4 reactants, suggesting that the reactants have considerable energy, perhaps in the form of electronic excitation.

What role do *f* orbitals play in metal ion chemistry?

As noted above, several ground state lanthanide cations (Ln^+) (Ln = Gd,[86, 87] Nd,[88] and Pr[89]) are oxidized by CO_2 to exhibit both an exothermic and prominent endothermic cross section feature. One question that arises in these studies is the role that the *f* orbitals play. In the exothermic reactions forming LnO^+ with CO_2, it can be realized that the ground state lanthanide cations do not have the appropriate atomic orbitals occupied to form the strong LnO^+ triple bond. The latter utilizes two *5d* orbitals on Ln coupled with the four *2p* electrons from the oxygen atom. Most Ln^+ ground states have a single *6s* orbital occupied with the remaining valence electrons in the *4f* orbitals. Gd^+ is an exception because the stability of the half-filled *4f* orbitals leads to a $4f^7 5d^1 6s^1$ ground state configuration. In all cases though, the surfaces evolving from ground state Ln^+ must couple with those evolving from an excited state having a ($4f^n 5d^2$) configuration in order to form ground state LnO^+ exothermically. This concept leads to the intriguing notion that the *f* orbitals can potentially play a role as both sources and sinks of electrons during such chemical reactions. In this regard, lanthanides, and by extension actinides (An), might be more versatile catalysts than transition metals because of such electronic flexibility. However, this requires that electrons can move readily from *f* orbitals into *d* orbitals when needed and vice versa when they are not. Such

transitions are parity forbidden spectroscopically, but is such coupling between orbitals facile during a reaction?

Two of our studies have begun to try to answer this question in a more quantitative way. In our study to determine the SmO^+ bond energy, we found that reaction 8 exhibited a barrier, even though our initial GIBMS[116] and subsequent photodissociation measurements[117] indicate the overall reaction is exothermic (by 0.143 ± 0.004 eV).

$$Sm^+ + CO_2 \rightarrow SmO^+ + CO \qquad (8)$$

Note that this observation contrasts with the exothermic and barrierless behavior noted above for the analogous reaction with Gd^+, Pr^+, and Nd^+. A more detailed study of process 8, its reverse, and of the $Sm^+(CO_2)$ and $OSm^+(CO)$ intermediates showed that the reverse of reaction 8 also exhibits a barrier, which is larger than the forward reaction by the exothermicity of reaction 8.[118] *Ab initio* calculations (Figure 8) indicated that this barrier corresponded to the crossing between the surfaces evolving from the ground state Sm^+ (^8F, $4f^6 6s^1$) + CO_2 ($^1\Sigma_g^+$) asymptote and that evolving from Sm^+ ($4f^5 5d^2$), which diabatically correlates with the ground state SmO^+ ($^6\Delta$) + CO ($^1\Sigma^+$) products. Thus, the overall reaction is spin-forbidden (as is also the case for the formation of GdO^+, PrO^+, and NdO^+ at low energies), but in this case, the crossing between the surfaces is measured to lie 1.77 ± 0.11 eV above ground state reactants, consistent with the minimum energy crossing point (MECP) calculated as 1.47 eV. The appreciable barrier is a result of the large excitation energy of the Sm^+ ($4f^5 5d^2$) state, 2.35 eV.[119] In contrast, the excitation energies for Gd^+, Pr^+, and Nd^+ are more modest at 0.55, 0.73, and 1.20 eV,[86-89] respectively, such that the comparable curve crossing can occur below the energy of the reactants.

Examination of the isovalent reaction of Sm^+ (^8F, $4f^6 6s^1$) with COS reveals a similar result for reaction 9.[120]

$$Sm^+ + COS \rightarrow SmO^+ + CS \qquad (9)$$

$$\rightarrow SmS^+ + CO \qquad (10)$$

Here, the reaction is endothermic by 1.28 ± 0.04 eV and yet the SmO^+ product is not observed until 2.8 ± 0.3 eV, 1.5 ± 0.3 eV above the thermodynamic threshold, Figure 9. Note that this excess

energy is comparable with the barrier observed in the CO_2 reaction, 1.8 ± 0.1 eV, and therefore we attribute it to the same origins, namely a crossing between the potential energy surfaces evolving from ground and excited state reactant asymptotes. Theory is consistent with this, although a specific MECP could not be located.

Contrasting with this behavior is the cross section for reaction 10, Figure 9. Now the reaction is exothermic by 0.23 ± 0.09 eV given $D_0(SmS^+)$ = 3.37 ± 0.09 eV.[121] In contrast to reaction 8, which is exothermic by a similar amount, reaction 10 proceeds with an efficiency of 26 ± 9% compared with the collision cross section calculated using the trajectory method that accounts for the dipole moment of COS.[122] This efficiency is invariant with kinetic energy (up to 0.4 eV), as measured by GIBMS cross sections (Figure 9), and or temperature (200 – 600 K), as determined by variable-temperature selected ion flow tube (VT-SIFT) rates. Note that the SmS^+ + CO product asymptote lies 1.5 ± 0.1 eV below the SmO^+ + CS asymptote, such that if the surface crossing drops by a similar amount, there is no longer a barrier (within the experimental uncertainty of ~0.4 eV), consistent with observation. At higher collision energy (above ~0.5 eV), the SmS^+ cross section increases to match the collision limit. This cross section feature can plausibly be assigned to formation of the spin-allowed SmS^+ ($^8\Gamma$) + CO ($^1\Sigma^+$) products, which are calculated to lie at an energy of 0.53 eV above ground state reactants. We concluded that the weakness of the OC-S bond coupled with the higher polarizability of the sulfur atom compared to oxygen allowed the system to create radical character more readily on the sulfur center compared to oxygen. This lowers the energy for formation of covalent bonds between Sm^+ and S, which also requires coupling with the sextet surface evolving from the excited Sm^+ ($4f^5 5d^2$) asymptote. Overall, we conclude that the ability of reaction systems to move electron density in and out of *f* orbitals is dependent on the details of the specific reaction involved and on the promotion energies associated with the electron configurations most conducive to bond formation.

Another question that arises in studies of Ln and An chemistry is whether *f* orbitals can participate directly in their reactions. In general, it is thought that the *4f* orbitals of the lanthanides are too compact to participate broadly in bonding, whereas the *5f* orbitals of the actinides can

participate, increasingly so as one moves to the right in the periodic table. Indeed, we have demonstrated the participation of *5f* orbitals in our measurements of the bond energies of ThO_2^+, $D_0(Th^+\text{-}O) = 8.57 \pm 0.14$ eV[123] and $D_0(OTh^+\text{-}O) = 4.94 \pm 0.06$ eV.[124] (Notably, the $ThO^+ + O_2$ endothermic reaction used to determine the latter bond energy has a $ThO_2^+ + O$ cross section that exhibits two distinct features. Here, entropic arguments were used to suggest enhanced formation of an electronically excited state of the ThO_2^+ product.) This thermochemistry was compared with that for the group 4 transition metal cations as they all have three valence electrons. TiO_2^+ and ZrO_2^+ both have second oxide bonds that are one-half of the first oxide bonds. This can be explained by the fact that these molecules have bent structures that utilize the *d* orbitals to form multiple metal-oxygen bonds. In the dioxides, the same set of *d* orbitals are shared by the two oxygen ligands, leading to the decrease in the bond energy. In contrast, calculations indicate that ThO_2^+ is a linear molecule, which has been demonstrated previously to indicate *f* orbital participation.[125, 126] Furthermore, we find that the second oxygen bond is 0.58 times as strong as the first oxygen bond, i.e., enhanced compared to the 0.50 factor found for the transition metals. Thus, *5f* orbital participation (five electrons in two π_u and one σ_u molecular orbitals) enhances the second oxygen bond by 1.5 eV (after accounting for the promotion energy needed to put Th^+ in the appropriate configuration for bonding), which is appreciable but still much weaker than the covalent bonds formed using the *6d* orbitals.

In contrast to their potential electronic flexibility, these heavy elements may have their reactivity restricted by their mere size. We have recently studied the reactions of Th^+ and U^+ with SF_6 and CF_4.[127, 128] Multiple fluorine and fluoride transfer reactions were observed at thermal energies in the SF_6 systems (yielding AnF_x^+ and SF_y^+ product ions) consistent with the exothermicity of these processes. In contrast, although comparable reactions are strongly exothermic for reaction with CF_4, both Th^+ and U^+ formed only AnF^+ at thermal energies with reaction efficiencies of only 0.1%. Additional fluorine and fluoride transfer reactions (yielding AnF_x^+ and CF_y^+ product ions) exhibited appreciable barriers (near 2 eV). The origins of this

behavior are not completely understood although we suggested that the short CF bonds did not permit facile activation by the relatively large actinide cations.

Conclusions

As alluded to above, although early work in my laboratory was able to study state-selected reactions of the *3d* transition metal cations, to date, no specific excited state chemistry has been explored for heavier (*4d*, *4f*, *5d*, *5f*) metals, except for Y^+ (^{1}S, ^{3}D), which we have studied with silane, Mo^+ (^{6}S, ^{4}G), which we have studied with methane,[129] and Au^+ (^{1}S, ^{3}D), which has been studied by Taylor and co-workers with methyl halides[130, 131] and my group with O_2 and N_2O.[132] In all cases, except Mo^+, variations in the ion source enabled different populations of the states to be generated and then quantitatively separated. Such a procedure does not work for most heavy elements because spin-orbit interactions interleave the different J levels of a single electronic term. Au^+ is an exception because the splitting of the ^{1}S and ^{3}D states is unusually large (>1.8 eV). Y^+ is an exception because the flow tube source generates a nearly pure beam of ground state ^{1}S whereas a surface ionization (SI) source makes mainly ^{3}D, with some contributions from ^{1}S and ^{1}D because the degeneracy of the ^{3}D state (15) is so much higher than ^{1}S (1). In the case of Mo^+, ion source variations (different electron ionization energies of $Mo(CO)_6$) were combined with ion mobility separation to compare the ^{6}S and ^{4}G states, both of which have $4d^5$ electron configurations. The ability of ion mobility to separate electronic states with different configurations[133] should be a valuable approach for many more heavy elements.

In all of these studies, it would be desirable to provide a more quantitative evaluation of spin-orbit coupling as one moves throughout the periodic table. As mentioned above, a quantitative predictive ability with regard to whether a system (both ground and excited electronic states) will behave diabatically or adiabatically is presently absent. Further, how these tendencies change with the energy or temperature of the system is needed and will provide better tests of the simple LZ model.

In this feature article, I pointed out that we have observed several interesting effects that are only evident when the kinetic energy of the system is varied over a wide range. In some cases, these can probably be identified as spin-forbidden versus spin-allowed reactions, but in other cases, changes in the qualitative nature of A′ versus A″ surfaces may be operative and in still others, an interesting orbital diabaticity may be in play. Clearly, it would be of interest to test our hypotheses with additional spectroscopic or reactive characterizations of the species formed at these high energies.

The oligomerization reactions first noted by Irikura and Beauchamp[7] deserve further attention because the ability to activate methane *and* then induce C-C coupling reactions is of technological importance. Several additional *5d* metals need to be compared with the already studied Pt^+ and Ir^+, to contrast and compare what kinds of products are feasible. Perhaps most intriguingly, the observation that under certain conditions an unreactive atomic element like Ru^+ can undergo these reactions indicates that many species and associated reaction conditions are worthy of further exploration.

Studies of the lanthanides and actinides as components of catalysts remain intriguing with regard to the role that the *f* orbitals play. More quantitative understanding of how strongly the *f* orbitals participate in bonding is needed. A better appreciation for limitations in the motility of electrons between different types of orbitals would be insightful.

The work suggested here could easily be extended to small metal clusters, which have been shown to exhibit changes (sometimes drastic) in their reactivity. The quantitative comparison of such gas-phase studies (for neutrals, cations, and anions) to ongoing work on single atoms and clusters deposited on substrates would be valuable. Such comparisons could elucidate the effects that the substrate has on the reactive species, as well as evaluate the charge state of the deposited species. Such insight could allow further developments in the overall reactivity and specificity of the catalytic processes.

Acknowledgement. I thank my students for their many contributions, which have been instrumental in the development of our research in this area. Our work has been generously funded by the National Science Foundation (most recently, CHE-2313553), the U.S. Department of Energy, Office of Basic Energy Sciences, Heavy Element Chemistry Program (most recently, DE-SC0012249), and the Air Force Office of Scientific Research (most recently, FA9550-20-1-0329).

References

1. Allison, J.; Ridge, D. P. Reactions of transition metal ions with alkyl halides and alcohols in the gas phase: evidence for metal insertion and .beta.-hydrogen atom shift. *J. Am. Chem. Soc.* **1976,** *98*, 7445-7447.

2. Allison, J.; Ridge, D. P. Reactions of atomic metal ions with alkyl halides and alcohols in the gas phase. *J. Am. Chem. Soc.* **1979,** *101*, 4998-5009.

3. Allison, J.; Freas, R. B.; Ridge, D. P. Cleavage of alkanes by transition metal ions in the gas phase. *J. Am. Chem. Soc.* **1979,** *101*, 1332-1333.

4. Davis, S. C.; Klabunde, K. J. Low temperature cleavage of alkanes by small nickel particles. Clustering of metal atoms in organic media. 7. *J. Am. Chem. Soc.* **1978,** *100*, 5973-5974.

5. Irikura, K. K.; Beauchamp, J. L. Osmium Tetroxide and Its Fragment Ions in the Gas Phase: Reactivity with Hydrocarbons and Small Molecules. *J. Am. Chem. Soc.* **1989,** *111*, 75-85.

6. Irikura, K. K.; Beauchamp, J. L. Electronic Structure Considerations for Methane Activation by Third-row Transition-metal Ions. *J. Phys. Chem.* **1991,** *95*, 8344-8351.

7. Irikura, K. K.; Beauchamp, J. L. Methane Oligomerization in the Gas Phase by Third-Row Transition-Metal Ions. *J. Am. Chem. Soc.* **1991,** *113*, 2769-2770.

8. Ranasinghe, Y. A.; MacMahon, T. J.; Freiser, B. S. Formation of Thermodynamically Stable Dications in the Gas Phase by Thermal Ion-Molecule Reactions: Ta^{2+} and Zr^{2+} with Small Alkanes. *J. Phys. Chem* **1991,** *95*, 7721-7726.

9. Armentrout, P. B.; Sievers, M. R. Activation of CH_4 by Gas-phase Zr^+ and the Thermochemistry of Zr ligand Complexes. *J. Phys. Chem. A* **2003,** *107*, 4396-4406.

10. Armentrout, P. B.; Beauchamp, J. L. The Chemistry of Atomic Transition Metal Ions: Insight into Fundamental Aspects of Organometallic Chemistry. *Accts. Chem. Res.* **1989,** *22*, 315-321.

11. Eller, K.; Schwarz, H. Organometallic Chemistry in the Gas Phase. *Chem. Rev.* **1991,** *91*, 1121-1177.

12. Weisshaar, J. C. Bare Transition Metal Atoms in the Gas Phase: Reactions of M, M^+ and M^{2+} with Hydrocarbons. *Acc. Chem. Res.* **1993,** *26*, 213-219.

13. Plattner, D. A., Metalorganic Chemistry in the Gas Phase: Insight into Catalysis. In *Modern Mass Spectrometry*, Schalley, C. A., Ed. Springer Berlin Heidelberg: Berlin, Heidelberg, 2003; pp 153-203.

14. Operti, L.; Rabezzana, R. Gas-phase ion chemistry in organometallic systems. *Mass Spectrom. Rev.* **2006,** *25*, 483-513.

15. Roithová, J.; Schröder, D. Selective Activation of Alkanes by Gas-Phase Metal Ions. *Chem. Rev.* **2010,** *110*, 1170–1211.

16. Schwarz, H. Chemistry with Methane: Concepts Rather than Recipes. *Angew. Chem. Int. Ed.* **2011,** *50*, 10096-10115.

17. Armentrout, P. B. Methane Activation by 5d Transition Metals: Energetics, Mechanisms, and Periodic Trends. *Chem.: Eur. J.* **2017,** *23*, 10-18.

18. Dietz, T. G.; Duncan, M. A.; Powers, D. E.; Smalley, R. E. Laser Production of Supersonic Metal Cluster Beams. *J. Chem. Phys.* **1981,** *74*, 6511-6512.

19. Bondybey, V. E.; English, J. H. Laser Induced Fluorescence of Metal Clusters Produced by Laser Vaporization: Gas Phase Spectrum of Pb_2. *J. Chem. Phys.* **1981,** *74*, 6978-6979.

20. Morse, M. D. Clusters of Transition Metal Atoms. *Chem. Rev.* **1986,** *86*, 1049-1109.

21. Armentrout, P. B. In *Transition Metal Cluster Ion Chemistry*, Laser Applications in Chemistry and Biophysics, El-Sayed, M., Ed. Proc. SPIE: 1986; p 38.

22. Castleman, A. W.; Harms, A. C.; Leuchtner, R. E. Gas phase reactivity of thermal metal clusters. *Zeitschrift für Physik D Atoms, Molecules and Clusters* **1991,** *19*, 343-346.

23. Luo, Z.; Castleman, A. W., Jr.; Khanna, S. N. Reactivity of Metal Clusters. *Chem. Rev.* **2016,** *116*, 14456-14492.

24. Luo, Z.; Khanna, S. N., An Overview of Metal Clusters and Their Reactivity. In *Metal Clusters and Their Reactivity*, Luo, Z.; Khanna, S. N., Eds. Springer Singapore: Singapore, 2020; pp 1-9.

25. Tyo, E. C.; Vajda, S. Catalysis by clusters with precise numbers of atoms. *Nat. Nanotechnol.* **2015,** *10*, 577-588.

26. Mitchell, S.; Pérez-Ramírez, J. Single atom catalysis: a decade of stunning progress and the promise for a bright future. *Nature Communications* **2020,** *11*, 4302.

27. Armentrout, P. B.; Hodges, R. V.; Beauchamp, J. L. Endothermic Reactions of Uranium Ions with N_2, D_2 and CD_4. *J. Chem. Phys.* **1977,** *66*, 4683-4688.

28. Ervin, K.; Loh, S. K.; Aristov, N.; Armentrout, P. B. Metal Cluster Ions: The Bond Energy of Mn_2^+. *J. Phys. Chem.* **1983,** *87*, 3593-3596.

29. Armentrout, P. B., Kinetic Energy Dependence of Ion Molecule Reactions: From Triatomics to Transition Metals. In *Structure/Reactivity and Thermochemistry of Ions*, Ausloos, P.; Lias, S. G., Eds. Reidel: Dordrecht, 1987; pp 97-164.

30. Armentrout, P. B. The Kinetic Energy Dependence of Ion-Molecule Reactions: Guided Ion Beams and Threshold Measurements. *Int. J. Mass Spectrom.* **2000,** *200*, 219-241.

31. Armentrout, P. B. Not Just a Structural Tool: The Use of Guided Ion Beam Tandem Mass Spectrometry to Determine Thermochemistry. *J. Am. Soc. Mass Spectrom.* **2002,** *13*, 419-434.

32. Armentrout, P. B. The Power of Accurate Energetics (or Thermochemistry: What is it Good for?). *J. Am. Soc. Mass Spectrom.* **2013,** *24*, 173-185.

33. Daly, N. R. Scintillation Type Mass Spectrometer Ion Detector. *Rev. Sci. Instrum.* **1960,** *31*, 264-267.

34. Teloy, E.; Gerlich, D. Integral Cross Sections for Ion-Molecule Reactions. 1. The Guided Beam Technique. *Chem. Phys.* **1974,** *4*, 417-427.

35. Houle, F. A.; Anderson, S. L.; Gerlich, D.; Turner, T.; Lee, Y. T. Nonadiabaticity in ion--molecule reactions: Coupling of proton and charge transfer in the H_2^+ and D_2^+ + Ar system. *J. Chem. Phys.* **1982,** *77*, 748-755.

36. Gerlich, D. Inhomogeneous rf Fields: A Versatile Tool for the Study of Processes with Slow Ions. *Adv. Chem. Phys.* **1992,** *82*, 1-176.

37. Ervin, K. M.; Armentrout, P. B. Translational Energy Dependence of $Ar^+ + XY \rightarrow ArX^+ + Y$ (XY = H_2, D_2, HD) from Thermal to 30 eV c.m. *J. Chem. Phys.* **1985,** *83*, 166-189.

38. Rodgers, M. T.; Ervin, K. M.; Armentrout, P. B. Statistical Modeling of Collision-Induced Dissociation Thresholds. *J. Chem. Phys.* **1997,** *106*, 4499-4508.

39. Rodgers, M. T.; Armentrout, P. B. Statistical Modeling of Competitive Threshold Collision-Induced Dissociation. *J. Chem. Phys.* **1998,** *109*, 1787-1800.

40. Armentrout, P. B. Statistical modeling of sequential collision-induced dissociation. *J. Chem. Phys.* **2007,** *126*, 234302.

41. Muntean, F.; Armentrout, P. B. Guided Ion Beam Study of Collision-Induced Dissociation Dynamics: Integral and Differential Cross Sections. *J. Chem. Phys.* **2001,** *115*, 1213-1228.

42. Armentrout, P. B., Thermochemical Measurements by Guided Ion Beam Mass Spectrometry. In *Adv. Gas Phase Ion Chem.*, Adams, N.; Babcock, L. M., Eds. JAI Press: Greenwich, Connecticut, 1992; Vol. 1, pp 83-119.

43. Elkind, J. L.; Armentrout, P. B. State-specific Reactions of Atomic Transition Metal Ions with H_2, HD and D_2: Effects of d Orbitals on Chemistry. *J. Phys. Chem.* **1987,** *91*, 2037-2045.

44. Schultz, R. H.; Armentrout, P. B. Reactions of N_4^+ with Rare Gases from Thermal to 10 eV c.m.: Collision-Induced Dissociation, Charge Transfer, and Ligand Exchange. *Int. J. Mass Spectrom. Ion Processes* **1991,** *107*, 29-48.

45. Schultz, R. H.; Crellin, K. C.; Armentrout, P. B. Sequential Bond Energies of $Fe(CO)_x^+$ (x = 1 - 5): Systematic Effects on Collision-Induced Dissociation Measurements. *J. Am. Chem. Soc.* **1991,** *113*, 8590-8601.

46. Elkind, J. L.; Armentrout, P. B. Does ground state Fe^+ react with H_2? *J. Am. Chem. Soc.* **1986,** *108*, 2765-2767.

47. Elkind, J. L.; Armentrout, P. B. Effect of Kinetic and Electronic Energy on the Reactions of Fe^+ with H_2, HD and D_2: State-Specific Cross Sections for $Fe^+(^6D)$ and $Fe^+(^4F)$. *J. Phys. Chem.* **1986,** *90*, 5736-5745.

48. Elkind, J. L.; Armentrout, P. B. Effect of Kinetic and Electronic Energy on the Reactions of Co^+, Ni^+ and Cu^+ with H_2, HD and D_2. *J. Phys. Chem.* **1986,** *90*, 6576-6586.

49. Schultz, R. H.; Armentrout, P. B. Nonadiabatic Behavior of a Transition Metal System: Exothermic Reactions of $Fe^+(^6D,^4F)$ and Propane. *J. Phys. Chem.* **1987,** *91*, 4433-4435.

50. Schultz, R. H.; Elkind, J. L.; Armentrout, P. B. Electronic Effects in C-H and C-C Bond Activation: State-specific Reactions of $Fe^+(^6D, ^4F)$ with Methane, Ethane and Propane. *J. Am. Chem. Soc.* **1988,** *110*, 411-423.

51. Langevin, P. Une Formule Fondamentale de Theorie Cinetique. *Ann. Chim. Phys. Ser. 8* **1905,** *5*, 245-288.

52. Gioumousis, G.; Stevenson, D. P. Reactions of Gaseous Molecule Ions with Gaseous Molecules. V. Theory. *J. Chem. Phys.* **1958,** *29*, 294-299.

53. Hanton, S. D.; Noll, R. J.; Weisshaar, J. C. Spin-orbit-level effect on iron(1+)(3d7,4FJ) + propane total reaction cross section at 0.22 eV. *J. Phys. Chem.* **1990,** *94*, 5655-5658.

54. Hanton, S. D.; Noll, R. J.; Weisshaar, J. C. Electronic-state-specific transition metal cation chemistry: $Fe^+ + C_3H_8$ and n-C_4H_{10}. *J. Chem. Phys.* **1992,** *96*, 5176-5190.

55. Elkind, J. L.; Armentrout, P. B. Effect of Kinetic and Electronic Energy on the Reaction of V^+ with H_2, HD and D_2. *J. Phys. Chem.* **1985,** *89*, 5626-5636.

56. Reents, W. D.; Strobel, F.; Freas, R. B.; Wronka, J.; Ridge, D. P. Chemical Reactions and Collisional Quenching of the Chromium Atomic Ion in a Metastable Excited State. *J. Phys. Chem* **1985,** *89*, 5666-5670.

57. Aristov, N.; Armentrout, P. B. Reaction Mechanisms and Thermochemistry of $V^+ + C_2H_{2p}$ (p = 1,2,3). *J. Am. Chem. Soc.* **1986,** *108*, 1806-1819.

58. Sunderlin, L.; Aristov, N.; Armentrout, P. B. Reaction of Scandium Ions with Ethane. First and Second Hydride Scandium Ion Bond Energies. *J. Am. Chem. Soc.* **1987,** *109*, 78-89.

59. Shaik, S.; Danovich, D.; Fiedler, A.; Schröder, D.; Schwarz, H. Two-State Reactivity in Organometallic Gas-Phase Ion Chemistry. *Helv. Chim. Acta* **1995,** *78*, 1393-1407.

60. Schröder, D.; Shaik, S.; Schwarz, H. Two-state Reactivity as a New Concept in Organometallic Chemistry. *Acc. Chem. Res.* **2000,** *33*, 139-145.

61. Schultz, R. H.; Armentrout, P. B. Threshold Collisional Activation of $Fe^+ \cdot C_3H_8$: Probing the Potential Energy Surface. *J. Am. Chem. Soc.* **1991,** *113*, 729-730.

62. Koppen, P. A. M. v.; Bowers, M. T.; Fisher, E. R.; Armentrout, P. B. Relative Energetics of C-H and C-C Bond Activation of Alkanes: Reactions of Ni+ and Fe+ with Propane on the Lowest Energy (Adiabatic) Potential Energy Surfaces. *J. Am. Chem. Soc.* **1994,** *116*, 3780-3791.

63. Holthausen, M. C.; Koch, W. Mechanistic Details of the Fe+-Mediated C□C and C□H Bond Activations in Propane: A Theoretical Investigation. *Helv. Chim. Acta* **1996,** *79*, 1939-1956.

64. Schwarz, H. On the spin-forbiddeness of gas-phase ion–molecule reactions: a fruitful intersection of experimental and computational studies. *Int. J. Mass Spectrom.* **2004,** *237*, 75-105.

65. Armentrout, M. M.; Li, F.-X.; Armentrout, P. B. Is Spin Conserved in Heavy Metal Systems? Experimental and Theoretical Studies of the Reaction of Re^+ with Methane. *J. Phys. Chem. A* **2004,** *108*, 9660-9672.

66. Kramida, A.; Ralchenko, Y.; Reader, J.; Team, N. A. NIST Atomic Spectra Database (ver. 5.7.1), [Online]. Available: http://physics.nist.gov/asd 2012. (accessed Nov 1, 2019).

67. Rue, C.; Armentrout, P. B.; Kretzschmar, I.; Schröder, D.; Harvey, J. N.; Schwarz, H. Kinetic-energy Dependence of Competitive Spin-allowed and Spin-forbidden Reactions: V^+ + CS_2. *J. Chem. Phys.* **1999,** *110*, 7858-7870.

68. Stowe, G. F.; Schultz, R. H.; Wight, C. A.; Armentrout, P. B. Translational and Electronic Energy Dependence of $S^+ + H_2(D_2,HD) \rightarrow SH^+(SD^+) + H(D)$. Spin-Allowed and Spin-Forbidden Pathways. *Int. J. Mass Spectrom. Ion Process.* **1990,** *100*, 177-195.

69. Sievers, M. R.; Armentrout, P. B. The Potential Energy Surface for Carbon-Dioxide Activation by V^+: A Guided Ion Beam Study. *J. Chem. Phys.* **1995,** *102*, 754-762.

70. Sievers, M. R.; Armentrout, P. B. Gas Phase Activation of Carbon Dioxide by Niobium and Niobium Monoxide Cations. *Int. J. Mass Spectrom.* **1998,** *179-180*, 103-115.

71. Rue, C.; Armentrout, P. B.; Kretzschmar, I.; Schröder, D.; Schwarz, H. Guided Ion Beam Studies of the State-Specific Reactions of Cr^+ and Mn^+ with CS_2 and COS. *Int. J. Mass Spectrom.* **2001,** *210/211*, 283-301.

72. Rue, C.; Armentrout, P. B.; Kretzschmar, I.; Schröder, D.; Schwarz, H. Guided Ion Beam Studies of the Reactions of Fe^+ and Co^+ with CS_2 and COS. *J. Phys. Chem. A* **2001,** *105*, 8456-8464.

73. Ruscic, B.; Pinzon, R. E.; Morton, M. L.; von Laszevski, G.; Bittner, S. J.; Nijsure, S. G.; Amin, K. A.; Minkoff, M.; Wagner, A. F. Introduction to Active Thermochemical Tables: Several "Key" Enthalpies of Formation Revisited. *J. Phys. Chem. A* **2004,** *108*, 9979-9997.

74. Ruscic, B.; Bross, D. H. Active Thermochemical Tables (ATcT) values based on ver. 1.124 of the Thermochemical Network. available at ATcT.anl.gov (accessed 10/18/22).

75. Johnson III, R. D. NIST Computational Chemistry Comparison and Benchmark Database. http://cccbdb.nist.gov/ (accessed Nov. 11, 2022).

76. Kretzschmar, I.; Schröder, D.; Schwarz, H.; Rue, C.; Armentrout, P. B. Experimental and Theoretical Studies of Vanadium Sulfur Cation. *J. Phys. Chem. A* **1998,** *102*, 10060-10073.

77. Zahr, G. E.; Preston, R. K.; Miller, W. H. Theoretical treatment of quenching in $O(^1D)$ + N_2 collisions. *J. Chem. Phys.* **1975,** *62*, 1127-1135.

78. Landau, L. Zur Theorie der Energieubertragung. II. *Physikalische Zeitschrift der Sowjetunion* **1932,** *2*, 46-51.

79. Zener, C. Non-adiabatic Crossing of Energy Levels. *Proc. R. Soc. London Ser. A* **1932,** *137*, 696-702.

80. Stueckelberg, E. C. G. Theorie der unelastischen Stösse zwischen Atomen. *Helvetica Physica Acta* **1932,** *5*, 369.

81. Baer, T.; Hase, W. L., *Unimolecular Reaction Dynamics: Theory and Experiments*. Oxford University Press: New York, 1996.

82. Tully, J. C., In *Dynamics of Molecular Collisions, Part B*, Miller, W. H., Ed. Plenum: New York, 1976.

83. Heller, E. J.; Brown, R. C. Radiationless Transitions in a New Light. *J. Chem. Phys.* **1983,** *79*, 3336-3351.

84. Lorquet, J. C.; Leyh-Nihant, B. Nonadiabatic unimolecular reactions. 1. A statistical formuation for the rate constants. *J. Phys. Chem.* **1988,** *92*, 4778-4783.

85. Dressler, R. A.; Arnold, S. T.; Murad, E. Charge-transfer Dynamics in Ion-polyatomic Molecule Collisions: $X^+ + H_2O$ (X = N, Kr) Luminescence Study. *J. Chem. Phys.* **1995,** *103*, 9989-10000.

86. Demireva, M.; Kim, J.; Armentrout, P. B. Gadolinium (Gd) Oxide, Carbide, and Carbonyl Cation Bond Energies and Evaluation of the $Gd + O \rightarrow GdO^+ + e^-$ Chemi-Ionization Reaction Enthalpy. *J. Phys. Chem. A* **2016,** *120*, 8550-8563.

87. Demireva, M.; Armentrout, P. B. Activation of CO_2 by Gadolinium Cation (Gd^+): Energetics and Mechanism from Experiment and Theory. *Top. Catal.* **2018,** *61*, 3-19.

88. Ghiassee, M.; Kim, J.; Armentrout, P. B. Evaluation of the Exothermicity of the Chemi-ionization Reaction $Nd + O \rightarrow NdO^+ + e^-$ and Neodymium Oxide, Carbide, Dioxide, and Carbonyl Cation Bond Energies. *J. Chem. Phys.* **2019,** *150*, 144309.

89. Ghiassee, M.; Stevenson, B. C.; Armentrout, P. B. Evaluation of the $Pr + O \rightarrow PrO^+ + e^-$ Chemi-ionization Reaction Enthalpy and Praseodymium Oxide, Carbide, Dioxide, and Carbonyl Cation Bond Energies. *Phys. Chem. Chem. Phys.* **2021,** *23*, 2938-2952.

90. Hinton, C. S.; Citir, M.; Armentrout, P. B. Guided Ion-Beam and Theoretical Studies of the Reaction of Os^+ (^6D) with O_2: Adiabatic and Nonadiabatic Behavior. *Int. J. Mass Spectrom.* **2013,** *354-355*, 87-98.

91. Armentrout, P. B. The Bond Energy of ReO^+: Guided Ion-Beam and Theoretical Studies of the Reaction of Re^+ (^7S) with O_2. *J. Chem. Phys.* **2013,** *139*, 084305.

92. Armentrout, P. B.; Li, F.-X. Bond Energy of IrO^+: Guided Ion-Beam and Theoretical Studies of the Reaction of Ir^+ (^5F) with O_2. *J. Phys. Chem. A* **2013,** *117*, 7754-7766.

93. Liu, Y.; Wang, L.; Lei, Y.; Suo, B.; Zhang, Y.; Zou, W. Theoretical study of low-lying electronic states of OsO^+. *Chem. Phys. Lett.* **2023,** *829*, 140692.

94. Ervin, K. M.; Armentrout, P. B. Spin-orbit State-selected Reactions of Kr^+($^2P_{3/2}$ and $^2P_{1/2}$) with H_2, D_2, and HD from Thermal Energies to 20 eV c.m. *J. Chem. Phys.* **1986,** *85*, 6380-6395.

95. Ervin, K. M.; Armentrout, P. B. Spin Orbit State selected Reactions of Xe^+($^2P_{3/2}$ and $^2P_{1/2}$) with H_2, D_2, and HD. *J. Chem. Phys.* **1989,** *90*, 118-126.

96. Kim, J.; Cox, R. M.; Armentrout, P. B. Guided Ion Beam and Theoretical Studies of the Reactions of Re^+, Os^+, and Ir^+ with CO. *J. Chem. Phys.* **2016,** *145*, 194305.

97. Kim, J.; Armentrout, P. B. Guided Ion Beam Tandem Mass Spectrometry and Theoretical Study of SO_2 Activated by Os^+ *J. Phys. Chem. A* **2020,** *124*, 6629-6644.

98. Kim, J.; Cox, R. M.; Armentrout, P. B. Thermochemical Studies of Reactions of Re^+ with SO_2 Using Guided Ion Beam Experiments and Theory. *Phys. Chem. Chem. Phys.* **2020,** *22*, 3191-3203.

99. Kim, J.; Armentrout, P. B. Thermochemistry of $Ir^+ + SO_2$ Reaction using Guided Ion Beam Tandem Mass Spectrometry and Theory. *J. Chem. Phys.* **2021,** *154*, 124302.

100. McNary, C. P.; Armentrout, P. B. Non-Adiabatic Behavior in the Homolytic and Heterolytic Bond Dissociation of Protonated Hydrazine: A Guided Ion Beam and Theoretical Investigation. *J. Chem. Phys.* **2017,** *147*, 124306.

101. Øiestad, E. L.; Uggerud, E. Unimolecular reactions of protonated hydrazine. Reaction mechanisms and dynamics from observation of metastable ion fragmentations and ab initio calculations. *Int. J. Mass Spectrom. Ion Processes* **1997,** *165-166*, 39-47.

102. Lapoutre, V. J. F.; Redlich, B.; van der Meer, A. F. G.; Oomens, J.; Bakker, J. M.; Sweeney, A.; Mookherjee, A.; Armentrout, P. B. Structures of the Dehydrogenation Products of Methane Activation by 5d Transition Metal Cations. *J. Phys Chem. A* **2013,** *117*, 4115-4126.

103. Armentrout, P. B.; Kuijpers, S.; Lushchikova, O.; Hightower, R. L.; Boles, G. C.; Bakker, J. M. Spectroscopic Identification of the Carbyne Hydride Structure of the Dehydrogenation Product of Methane Activation by Osmium Cations. *J. Am. Soc. Mass Spectrom.* **2018,** *29*, 1781-1791.

104. Owen, C. J.; Boles, G. C.; Chernyy, V.; Bakker, J. M.; Armentrout, P. B. Structures of the Dehydrogenation Products of Methane Activation by 5d Transition Metal Cations Revisited: Deuterium Labeling and Rotational Contours. *J. Chem. Phys.* **2018,** *148*, 044307.

105. Aguirre, F.; Husband, J.; Thompson, C. J.; Metz, R. B. Gas-phase Photodissociation of $AuCH_2^+$: The Dissociation Threshold of Jet-cooled and Rotationally Thermalized Ions. *Chem. Phys. Lett.* **2000,** *318*, 466-470.

106. Armentrout, P. B.; Stevenson, B. C.; Yang, F.; Wensink, F. J.; Lushchikova, O. V.; Bakker, J. M. Infrared Spectroscopy of Gold Carbene Cation ($AuCH_2^+$): Covalent or Dative Bonding? *J. Phys. Chem. A* **2019,** *123*, 8932-8941.

107. Irikura, K. K.; Goddard III, W. A. Energetics of Third-Row Transition Metal Methylidene Ions MCH_2^+ (M = La, Hf, Ta, W, Re, Os, Ir, Pt, Au). *J. Am. Chem. Soc.* **1994,** *116*, 8733-8740.

108. Heinemann, C.; Hertwig, R. H.; Wesendrup, R.; Koch, W.; Schwarz, H. Relativistic Effects on Bonding in Cationic Transition-Metal-Carbene Complexes: A Density-Functional Study. *J. Am. Chem. Soc.* **1995,** *117*, 495-500.

109. de Macedo, L. G. M.; Pyykkö, P. Bonding trends in MCH_2 systems: Simple orbital interpretation and evidence for double bonds. *Chem. Phys. Lett.* **2008,** *462*, 138-143.

110. Zhang, X.; Schwarz, H. Bonding in Cationic MCH_2^+ (M=K–La, Hf–Rn): A Theoretical Study on Periodic Trends. *Chem. Eur. J.* **2010,** *16*, 5882 – 5888.

111. Wheeler, O. W.; Salem, M.; Gao, A.; Bakker, J. M.; Armentrout, P. B. Activation of C-H bonds in $Pt^+ + xCH_4$ Reactions, Where x = 1 – 4: Identification of the Platinum Dimethyl Cation. *J. Phys. Chem. A* **2016,** *120*, 6216–6227.

112. Wensink, F. J.; Roos, N.; Bakker, J. M.; Armentrout, P. B. C–H Bond Activation and C–C Coupling of Methane on a Single Cationic Platinum Center: A Spectroscopic and Theoretical Study. *Inorg. Chem.* **2022,** *61*, 11252-11260.

113. Wheeler, O. W.; Salem, M.; Gao, A.; Bakker, J. M.; Armentrout, P. B. Sequential Activation of Methane by Ir^+: An IRMPD and Theoretical Investigation. *Int. J. Mass Spectrom.* **2019,** *435*, 78-92.

114. Wensink, F. J.; Pradeep, D.; Armentrout, P. B.; Bakker, J. M. IR spectroscopic characterization of products of methane and cyclopropane activation by Ru cations. *Int. J. Mass Spectrom.* **2023**, 117165.

115. Armentrout, P. B.; Chen, Y.-M. Activation of Methane by Ru^+: Experimental and Theoretical Studies of the Thermochemistry and Mechanism. *Int. J. Mass Spectrom.* **2016,** *413*, 135-149.

116. Cox, R. M.; Kim, J.; Armentrout, P. B.; Bartlett, J.; VanGundy, R. A.; Heaven, M. C.; Ard, S. G.; Melko, J. J.; Shuman, N. S.; Viggiano, A. A. Evaluation of the Exothermicity of the Chemi-ionization Reaction Sm + O → $SmO^+ + e^-$. *J. Chem. Phys.* **2015,** *142*, 134307.

117. Lachowicz, A.; Perez, E.; Shuman, N. S.; Ard, S. G.; Viggiano, A. A.; Armentrout, P. B.; Goings, J.; Sharma, P.; Li, X.; Johnson, M. Determination of the SmO^+ Bond Energy by Threshold Photodissociation of the Cryogenically Cooled Ion. *J. Chem. Phys.* **2021,** *155*, 174303.

118. Armentrout, P. B.; Cox, R. M. Potential Energy Surface for Reaction of $Sm^+ + CO_2 \rightarrow SmO^+ + CO$: Guided Ion Beam and Theoretical Studies. *Phys. Chem. Chem. Phys.* **2017,** *19*, 11075-11088.

119. Gibson, J. K. Role of Atomic Electronics in f-Element Bond Formation: Bond Energies of Lanthanide and Actinide Oxide Molecules. *J. Phys. Chem. A* **2003,** *107*, 7891-7899.

120. Armentrout, P. B.; Cox, R. M.; Sweeny, B. C.; Ard, S. G.; Shuman, N. S.; Viggiano, A. A. Lanthanides as Catalysts: Guided Ion Beam and Theoretical Studies of $Sm^+ + COS$. *J. Phys. Chem. A* **2018,** *122*, 737-749.

121. Armentrout, P. B.; Demireva, M.; Peterson, K. A. Guided Ion Beam and Theoretical Studies of the Bond Energy of SmS^+. *J. Chem. Phys.* **2017,** *147*, 214307.

122. Su, T.; Chesnavich, W. J. Parameterization of the Ion-polar Molecule Collision Rate Constant by Trajectory Calculations. *J. Chem. Phys.* **1982,** *76*, 5183-5185.

123. Cox, R. M.; Citir, M.; Armentrout, P. B.; Battey, S. R.; Peterson, K. A. Bond Energies of ThO^+ and ThC^+: A Guided Ion Beam and Quantum Chemical Investigation of the Reactions of Thorium Cation with O_2 and CO. *J. Chem. Phys.* **2016,** *144*, 184309.

124. Armentrout, P. B.; Peterson, K. A. Guided Ion Beam and Quantum Chemical Investigation of the Thermochemistry of Thorium Dioxide Cations: Thermodynamic Evidence for Participation of *f* Orbitals in Bonding. *Inorg. Chem.* **2020,** *59*, 3118-3131.

125. Wadt, W. R. Why UO_2^{2+} is Linear and Isoelectronic ThO_2 is Bent. *J. Am. Chem. Soc.* **1981,** *103*, 6053-6057.

126. Dyall, K. G. Bonding and bending in the actinyls. *Molec. Phys.* **1999,** *96*, 511-518.

127. Bubas, A. R.; Iacovino, A. C.; Armentrout, P. B. Reactions of Atomic Thorium and Uranium Cations with SF_6 Studied by Guided Ion Beam Tandem Mass Spectrometry. *J. Phys. Chem. A* **2022,** *20*, 3239-3246.

128. Bubas, A. R.; Owen, C. J.; Armentrout, P. B. Reactions of Atomic Thorium and Uranium Cations with CF_4 Studied by Guided Ion Beam Tandem Mass Spectrometry. *Int. J. Mass Spectrom.* **2022,** *472*, 116778.

129. Armentrout, P. B., Electronic State Chromatography: Ion Mobility of Atomic Cations and Their Electronic States. In *Ion Mobility Spectroscopy - Mass Spectrometry: Theory and Applications*, Wilkins, C.; Trimpin, S., Eds. CRC Press: Boca Raton, 2011; pp 31-51.

130. Taylor, W. S.; May, J. C.; Lasater, A. S. Reactions of $Cu^+(^1S,^3D)$ and $Au^+(^1S,^3D)$ with CH_3Br. *J. Phys. Chem. A* **2003,** *107*, 2209-2215.

131. Taylor, W. S.; Matthews, C. C.; Hicks, A. J.; Fancher, K. G.; Chen, L. C. Near-Thermal Reactions of $Au^+(^1S,^3D)$ with CH_3X (X = F,Cl). *J. Phys. Chem. A* **2012,** *116*, 943–951.

132. Li, F.-X.; Gorham, K.; Armentrout, P. B. Oxidation of Atomic Gold Ions: Thermochemistry for the Activation of O_2 and N_2O by Au^+ ($^1S_0$ and ^3D). *J. Phys. Chem. A* **2010,** *114*, 11043–11052

133. Kemper, P. R.; Bowers, M. T. Electronic-state Chromatography: Application to First Row Transition-Metal Ions. *J. Phys. Chem* **1991,** *95*, 5134-5146.

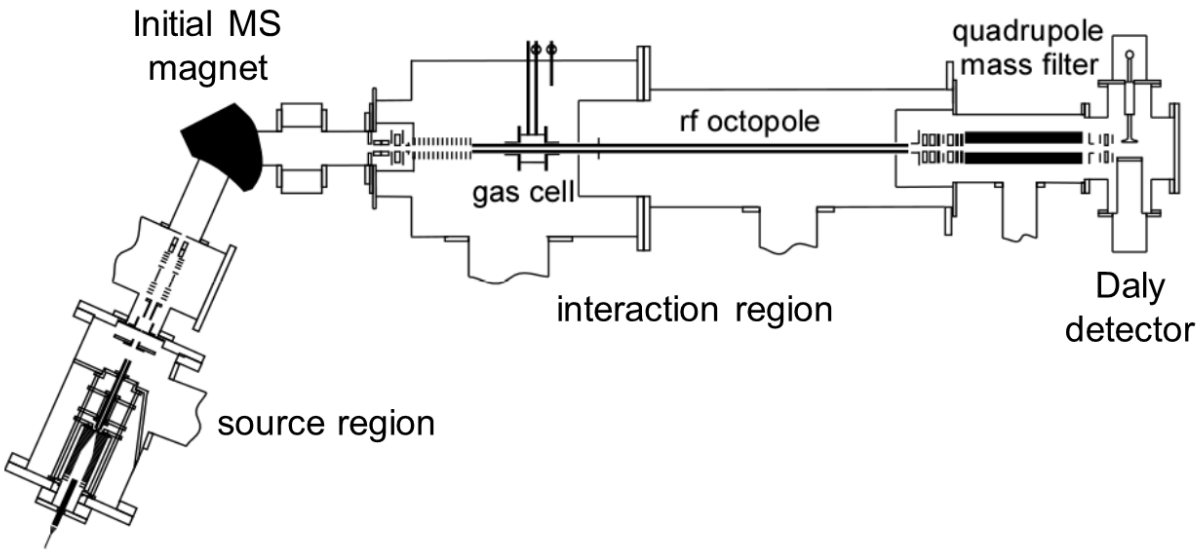

Figure 1. A schematic of one of our GIBMS instruments showing the major components. Shown for the source is an electrospray ionization, rf ion funnel, rf hexapole source. Pumping is indicated by the ports with wavy lines.

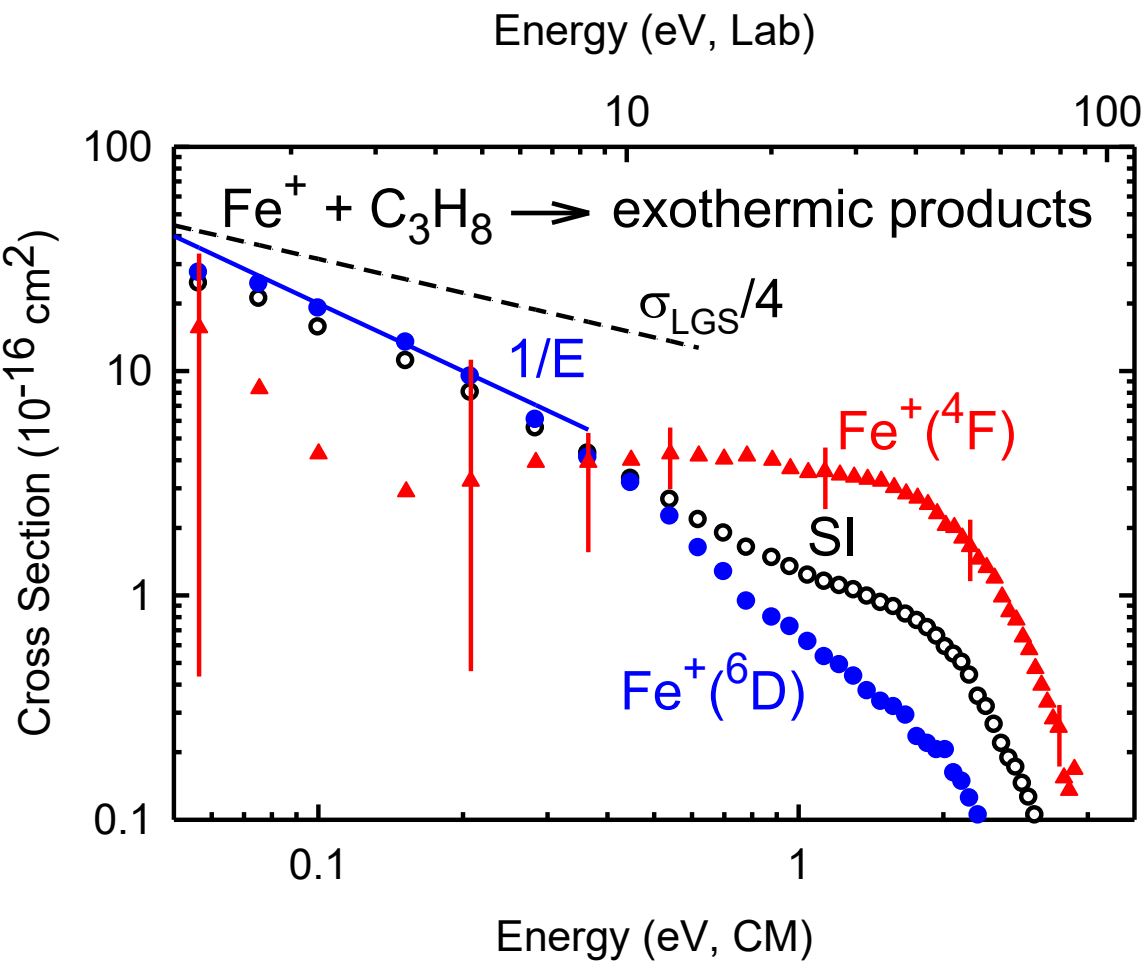

Figure 2. Cross sections for exothermic reactions of Fe^+ and propane as a function of kinetic energy in the center-of-mass (lower scale) and laboratory (upper scale) frames. Symbols show results for $Fe^+(^6D)$ (blue circles) and $Fe^+(^4F)$ (red triangles). Open black symbols show results for Fe^+ produced in the surface ionization (SI) source. The dashed line shows σ_{LGS} divided by 4 and the full blue line shows an energy dependence of E^{-1}. Vertical bars show approximate uncertainties in the derived cross sections for reaction of $Fe^+(^4F)$. Adapted with permission from ref. [49]. Copyright 1987 ACS.

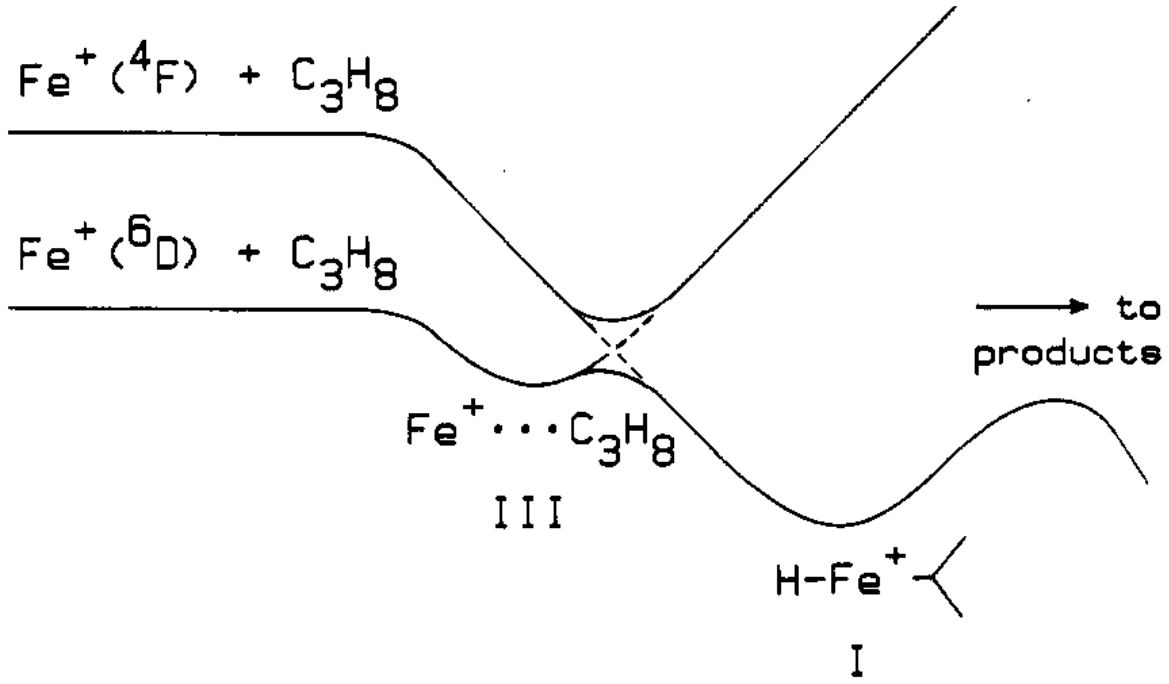

Figure 3. Qualitative potential energy surfaces for the state-specific reaction of Fe^+ and propane. Full lines represent the adiabatic surfaces while dashed lines show the quartet and sextet diabatic surfaces. Reproduced with permission from ref. [49]. Copyright 1987 ACS.

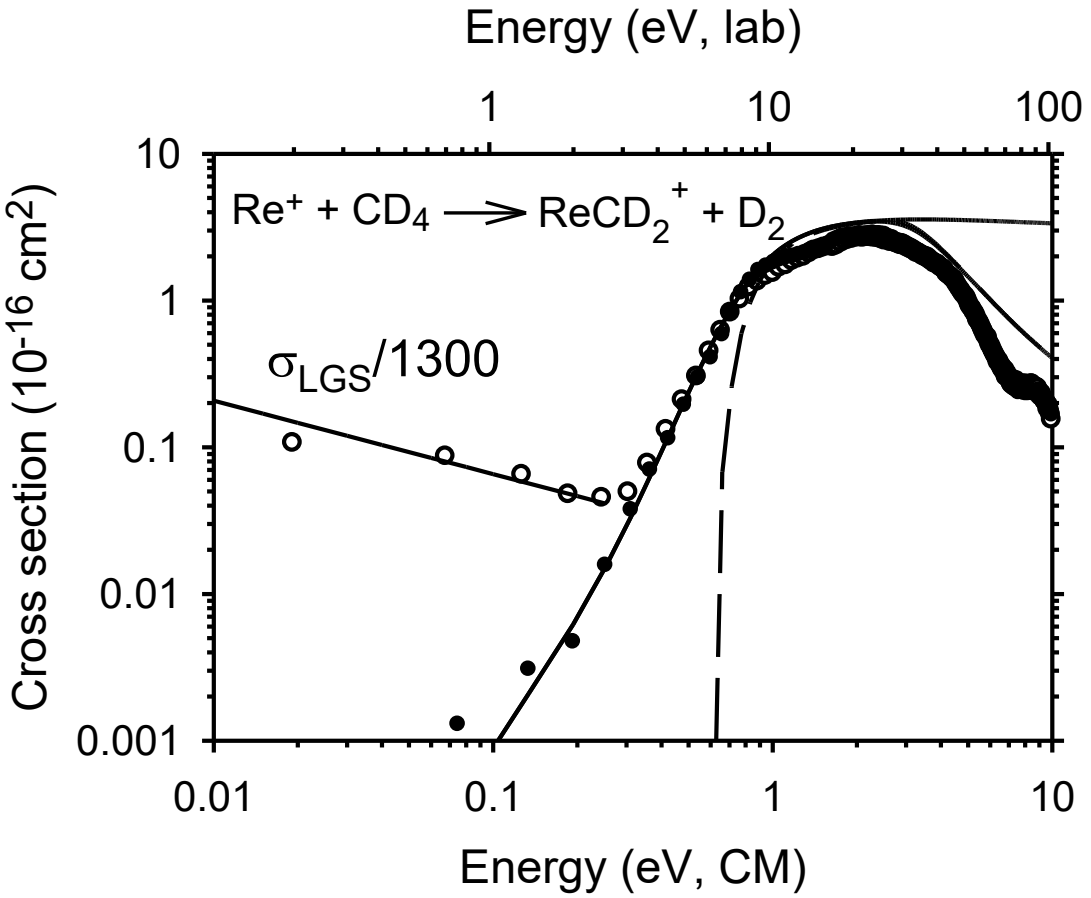

Figure 4. Cross sections for the dehydrogenation reaction of Re^+ with CD_4 as a function of kinetic energy in the center-of-mass frame (lower axis) and laboratory frame (upper axis). Results are shown for Re^+ produced without (open circles) and with (closed circles) methane added to the flow tube source. At low energy, the line shows the LGS collision cross section scaled down by a factor of 1300. At higher energies, the lines are the results of phase space calculations (PSC) including (solid lines) and excluding (dashed line) the kinetic and internal energy distributions of the reactant neutral and ion. Above ~3 eV, the two lines show the PSC with (lower line) and without (upper line) competition with formation of $ReD^+ + CD_3$. Reproduced with permission from ref. [65]. Copyright 2004 ACS.

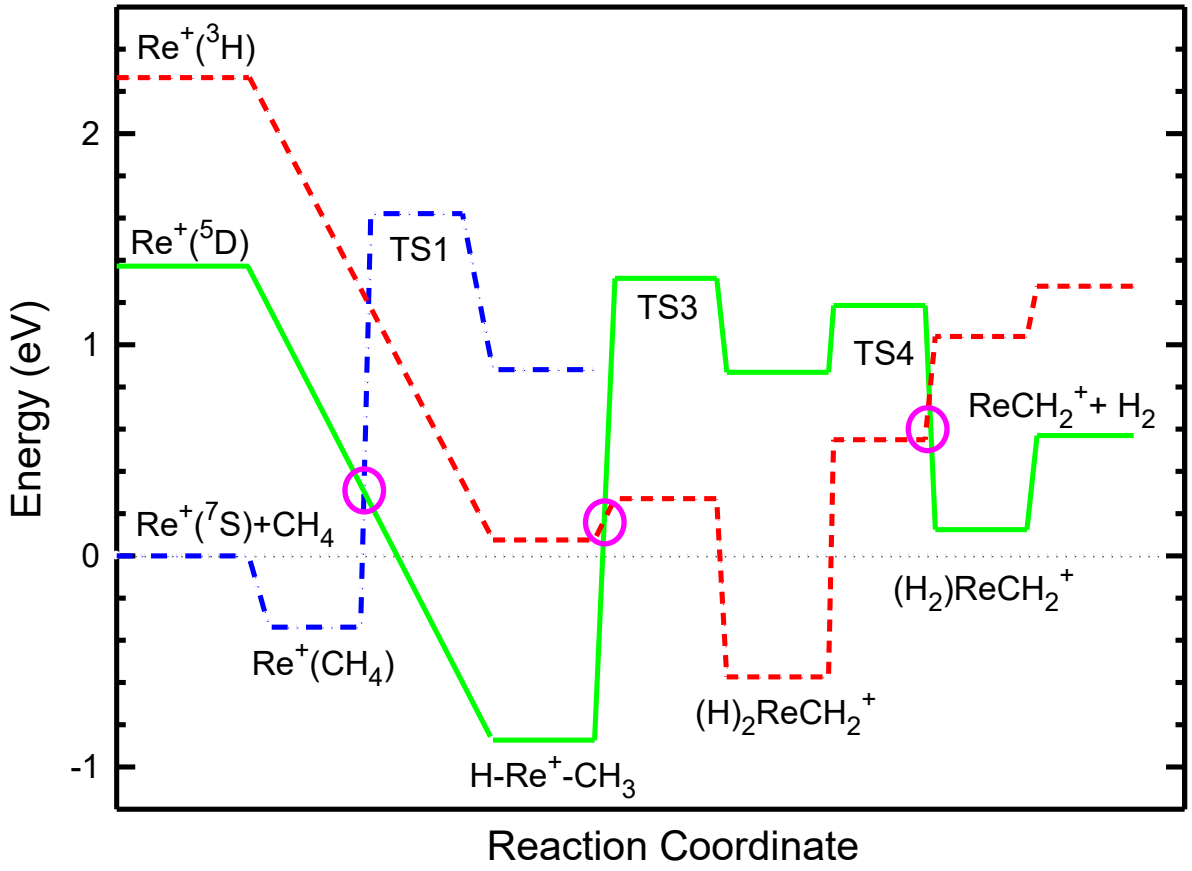

Figure 5. $[ReCH_4]^+$ potential energy surfaces (blue dash-dot, green solid, and red dashed lines for septet, quintet, and triplet spin, respectively) derived from theoretical results except for the ground state product asymptote, which is experimental. Circles indicate approximate crossing points between surfaces. Adapted with permission from ref. [65]. Copyright 2004 ACS.

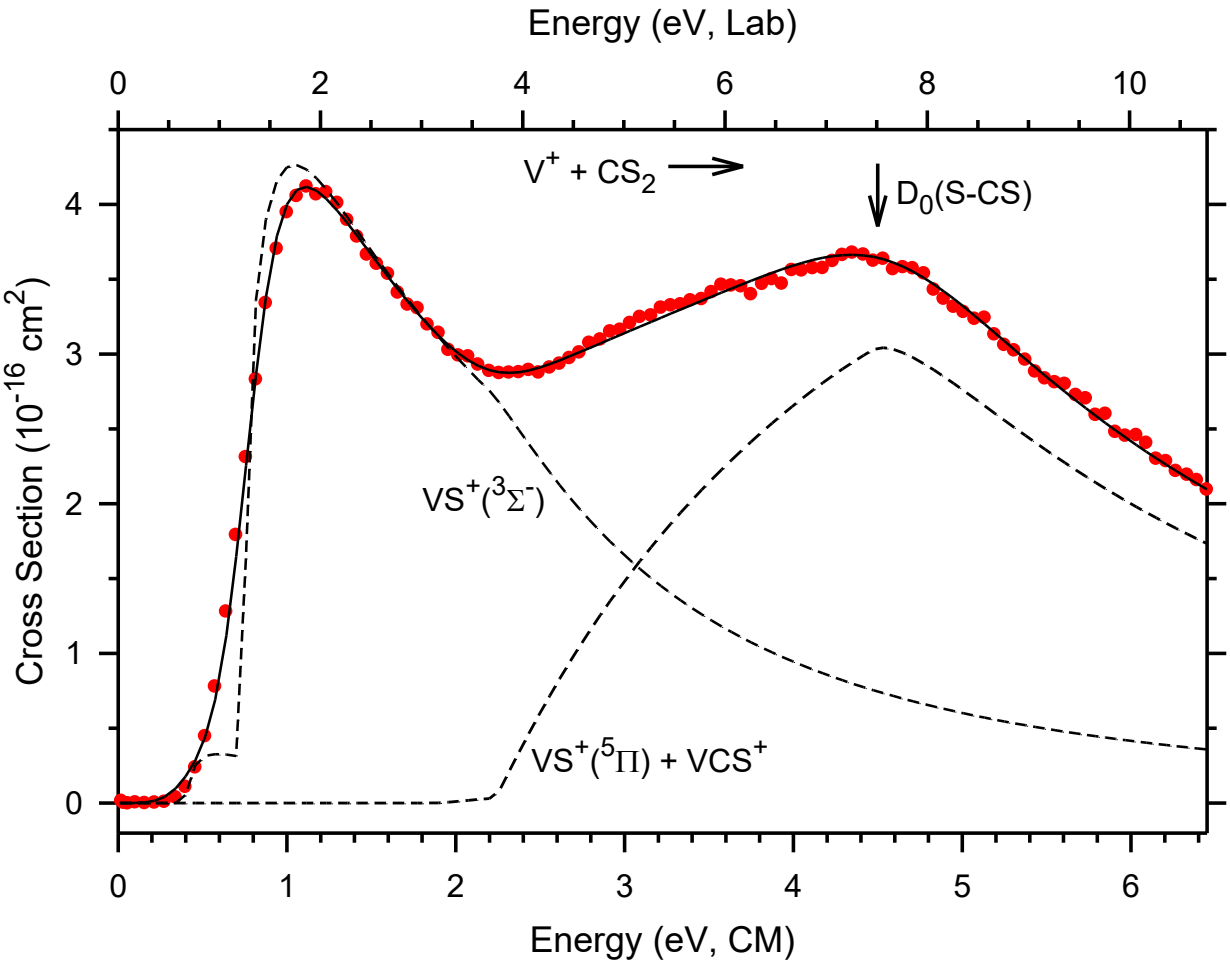

Figure 6. Total cross section (symbols) for reaction of V^+ with CS_2 as a function of kinetic energy in the center-of-mass (lower axis) and laboratory (upper axis) frames. The estimated 0 K cross sections for formation of VS^+ ($^3\Sigma^-$) and the sum of VS^+ ($^5\Pi$) + VCS^+ are shown by the broken lines. The full line shows the sum of these after convolution over the experimental internal and kinetic energy distributions. At threshold, the dashed lines show contributions from both the V^+ (^{5}F) excited state and V^+ (^{5}D) ground state. The vertical arrow indicates the bond energy of CS_2 at 4.50 eV. Adapted with permission from ref. [67]. Copyright 1999 AIP.

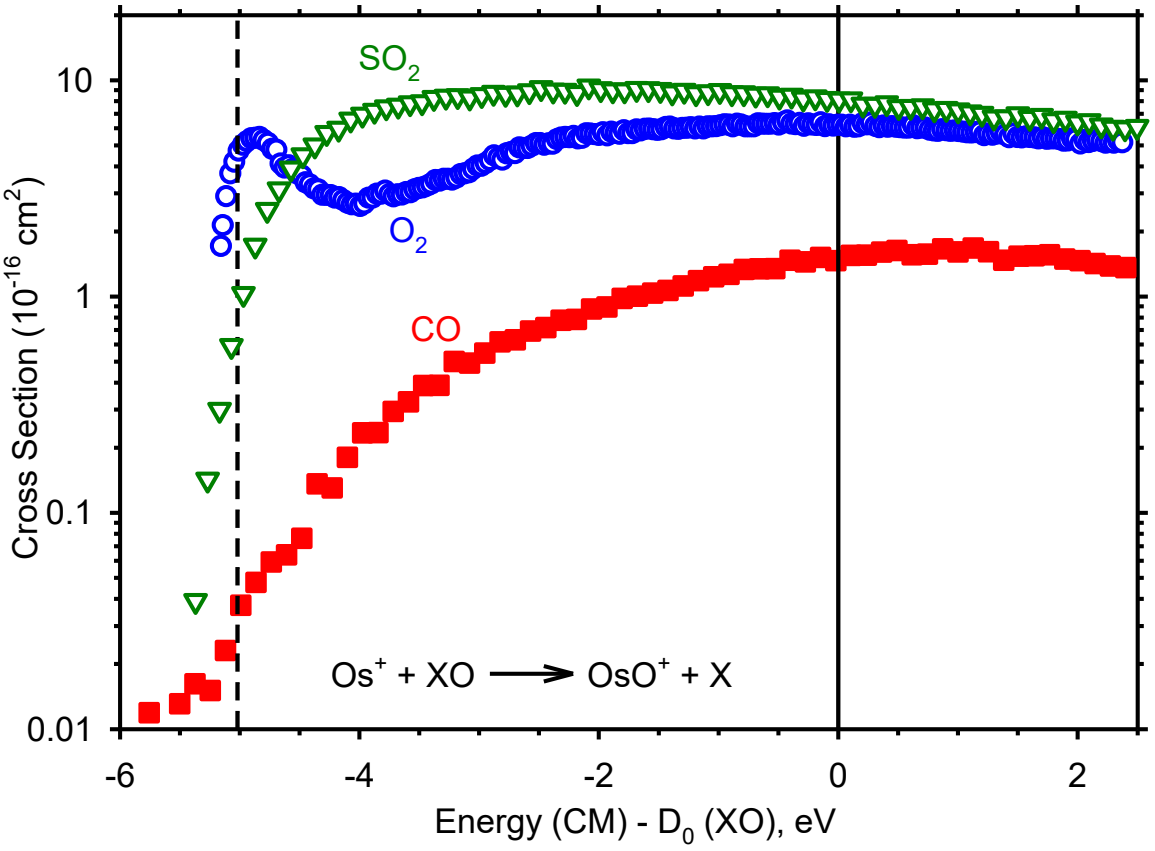

Figure 7. Product cross sections for the reactions of SO_2 (green inverted triangles), O_2 (blue circles), and CO (red squares) with Os^+ (^6D) as a function of the center-of-mass frame energy minus the BDE of the neutral reactant (solid vertical line), which aligns the threshold energy for all three systems (dashed vertical line). Adapted with permission from ref. [97]. Copyright 2020 ACS.

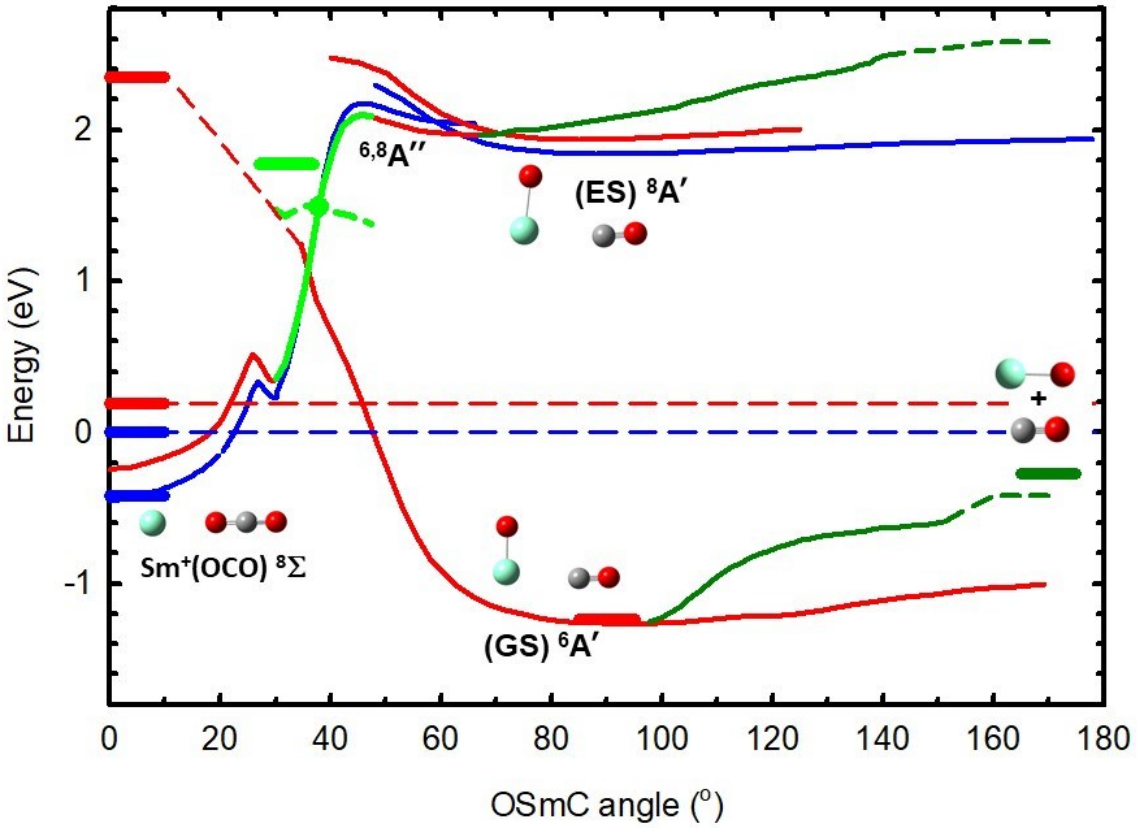

Figure 8. Potential energy surfaces as a function of the OSmC bond angle for the reaction of Sm^+ with CO_2 corrected for the SO splitting of the $^8F_{1/2}$ level. Red and blue lines indicate surfaces of sextet and octet spin, respectively. Thick short horizontal lines indicate experimentally determined energies. Dark green lines show dissociation to the SmO^+ + CO asymptotes, with the dashed portions no longer corresponding accurately to the OSmC bond angle. The dashed light green line shows the sextet surface for an electron configuration with five *4f* electrons at the same geometries as those with six *4f* electrons (solid light green line). The minimum energy crossing point (MECP) is indicated by the green circle. Adapted with permission from ref. [120]. Copyright 2018 ACS.

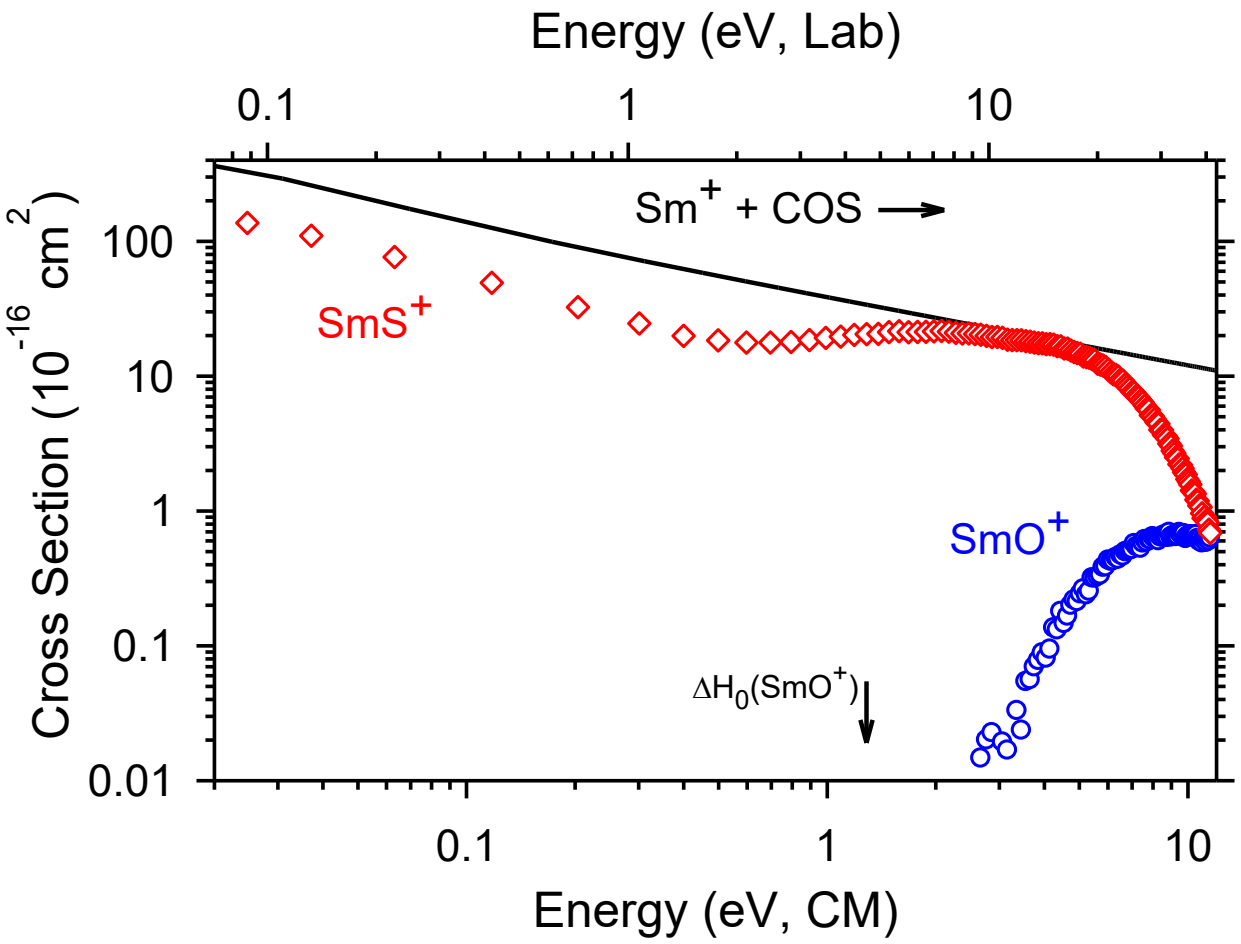

Figure 9. Cross sections for the reaction between Sm^+ and COS as a function of energy in the center-of-mass (lower x-axis) and laboratory (upper x-axis) frames. The solid black line shows the collision cross section calculated using the trajectory model of ref. [122]. The vertical arrow indicates the thermodynamic threshold for SmO^+ + CS formation at 1.28 eV. Adapted with permission from ref. [120]. Copyright 2018 ACS.

TOC Graphic

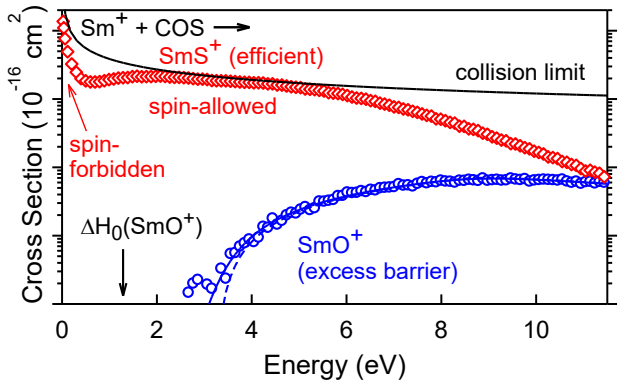
Sm+ + COS
SmS+ (efficient)
collision limit
spin-allowed
spin-
forbidden
ΔH0(SmO+)
SmO+
(excess barrier)
Cross Section (10-16 cm2)
0
2
4
6
8
10
Energy (eV)

Author Biography. P. B. Armentrout, Department of Chemistry, University of Utah, Utah, USA. Some 40 years ago, Professor Armentrout and his group developed the first guided ion beam tandem mass spectrometer to quantitatively examine the kinetic energy dependence of ion–molecule reactions. In the interim, he and his group have developed sophisticated tools to analyze the resultant reaction cross sections and provide thermodynamic, kinetic, and dynamic information on a wide range of chemical species. Innovative use of a variety of ion sources has extended the applicability of these methods to a host of interesting inorganic and biological molecules. His group is well-known for providing quality thermodynamic information for species ranging from diatomic molecules, to atomic clusters, to solvated systems, and biopolymers. Professor Armentrout is currently Distinguished Professor and Henry Eyring Presidential Endowed Chair of Chemistry at the University of Utah, where he has taught since 1987. He has been recognized by a number of awards and his research is documented in over 570 refereed articles and book chapters.